Applied Catalysis B: Environmental 328 (2023) 122491

Contents lists available at ScienceDirect

Applied Catalysis B: Environmental

journal homepage: www.elsevier.com/locate/apcatb

Highly-efficient conversion of lignin to electricity by nickel foam anode loaded with solid electrocatalysts

Denghao Ouyang [a,b], Daihong Gao [a,b], Ye Qiang [a,b], Xuebing Zhao [a,b,*]

[a] Key Laboratory of Industrial Biocatalysis, Ministry of Education, Tsinghua University, Beijing 100084, China
[b] Institute of Applied Chemistry, Department of Chemical Engineering, Tsinghua University, Beijing 100084, China

ARTICLE INFO

Keywords:
Lignin
Electricity generation
Solid electrocatalyst
Liquid flow fuel cell
Electron transfer

ABSTRACT

A novel liquid flow fuel cell with insoluble metal sulfides-modified nickel foam anodes was developed to achieve direct conversion of lignin to electricity under mild conditions, avoiding the separation problems caused by using soluble electron mediators. CoS has been screened as the most efficient anodic electrocatalyst for lignin oxidation in alkaline medium by Co^{2+}/Co^{3+} redox couple. By using an alkaline anolyte-acidic catholyte asymmetric design with VO^{2+}/VO_2^+ redox couple as the cathodic electrocatalysts, the highest peak power density of 176 mW/cm^2 was obtained with sodium lignosulfonate as the fuel at 80 ℃. The anode showed excellent stability with a 97% selectivity over oxygen evolution reaction for at least four fed-batch operation without significant loss of the activity. Lignin underwent significant depolymerization and degradation primarily by cleavage of β-O-4′ aryl ether bond, while ring-opening reactions also took place to form aliphatic acids, and even a part of lignin was mineralized to CO_2.

1. Introduction

Depletion of fossil resource and environmental problems caused by large-scale combustion of fossil fuels have urgently driven people to use renewable sources for sustainable production of power. Biomass such as lignocellulose usually available as agricultural residues has been considered as one of the most promising renewable feedstock for production of biofuels, materials and electricity, because of its features of abundance and carbon neutrality. As the second most abundant organic material in natural world, utilization of lignin has been paid more and more attention in recent years [1]. Compared with the polysaccharide components of lignocellulose, namely cellulose and hemicelluloses, lignin that is usually produced as a by-product in pulping industry and lignocellulose biorefinery, has higher carbon content and is an ideal fuel for electricity generation, either by combustion to drive steam turbine or fueling fuel cells.

Liquid flow fuel cells (LFFCs) present a state-of-art electricity generation technology with high exergy efficiency and low environmental impact [2]. Particularly, LFFCs fueled with various biomass fuel including lignin, also known as direct biomass fuel cells (DBFCs), is an emerging technology. However, direct conversion of lignin to electricity under mild condition is challenging, because of the recalcitrant structure of lignin to degradation by oxygen under mild conditions. Therefore, to promote the kinetics of electron transfer, bioinspired electron transport chains (ETCs) have been constructed with redox couples as the electron mediators to increase the rate of electron transfer from the "fuel" to oxygen thus achieving great improvement of the power density [3]. In anodic reactions, the electron mediators oxidize the fuels and then release the electrons to anode thus increasing the kinetics of fuel oxidation. Currently, several anodic electron mediators have been screened, such as polyoxometalates (POMs) including phosphomolybdic acid [4], molybdovanadophosphoric heteropoly acids [5], and silicotungstic acid [6]; organic electron mediators including anthraquinone-2-sulfonic acid [7], methylene blue [8] and methyl viologen [9], and ferric salts such as $FeCl_3$ [10] and ferricyanides [11]. For the cathode side, several redox couples have been employed as mediators to promote the kinetics of O_2 reduction, such as $(VO_2)_2SO_4$ [11], POMs [12], $Fe(NO_3)_3$ [13] and HNO_3 [14]. The use of liquid electron mediators in catholyte can efficiently transform the traditional gas-liquid-solid three-phase reaction catalyzed by solid catalyst for oxygen reduction reaction (ORR) into gas-liquid two-phase reaction, which thus greatly reduces the mass transfer resistance and increases the rate of electron transfer [15]. However, in the anolyte, the anodic electron mediators usually cannot quantitatively oxidize lignin to CO_2

* Corresponding author at: Key Laboratory of Industrial Biocatalysis, Ministry of Education, Tsinghua University, Beijing 100084, China.
E-mail address: zhaoxb@mail.tsinghua.edu.cn (X. Zhao).

https://doi.org/10.1016/j.apcatb.2023.122491
Received 31 August 2022; Received in revised form 9 January 2023; Accepted 18 February 2023
Available online 20 February 2023

because of the robustness of C-C bond, particularly under mild conditions. For example, Liu et al. developed a LFFC with phosphomolybdic acid as the anodic electron mediators and molybdovanadophosphoric heteropoly acids as the cathodic electron mediator. They estimated that 88% of the initial glucose, 82% of the cellulose, and 65% of the lignin were converted into CO_2, suggesting that there were still unreacted fuel and small-molecule degradation products in anolyte [16]. Zu et al. investigated that the decomposition reaction of glucose oxidized by $FeCl_3$. Under the optimized conditions, CO_2 was detected in the collected gaseous products, indicating the cleavage of C-C bond. However, they also detected the presence of typical intermediate products such as formic acid, acetic acid and 4- hydroxybutyric acid in the anolyte [10]. It should be noted that these intermediates can be further oxidized by anodic electron mediators to CO_2. However, during a long-term discharging, the degradation products may accumulate gradually, which may reduce the performance of the cell. Hence, the anolyte should be further refreshed and the liquid anodic electron mediators need to be separated and recovered from the degradation product mixture. However, currently the used anodic electron mediators are soluble in the aqueous anolyte and it is usually difficult to recover. Therefore, easily-recoverable anode electron mediators should be developed for lignin-fueled LFFCs. These issues have driven us to develop solid electron mediators or electrocatalysts for anodic reaction to achieve direct conversion of lignin to electricity under mild conditions. Nevertheless, the success of such a solid anodic electrocatalyst-based electron transport chain (ETC) necessitates the improvement of the efficiency of electron and mass transfer between the mediators and lignin, investigation of the kinetics of electron transfers as well as understanding the mechanisms of lignin degradation. Therefore, aiming to solve the above issues, the objective of this work is to develop a new LFFC system equipped with a solid electrocatalyst-modified anode in alkaline anolyte for efficient conversion of lignin to electricity under mild conditions (below 100 ℃), which can avoid the steps of separation and recovery of the catalyst caused by using liquid electron mediators. This work thus may make a novel step forward to large-scale application of lignin-fueled LFFCs.

2. Materials and methods

2.1. Chemicals and materials

All the chemicals used in the experiments including cobalt chloride ($CoCl_2$), thiourea, absolute ethyl alcohol, vanadium pentoxide (V_2O_5), potassium hydroxide (KOH), sulfuric acid (H_2SO_4), nitric acid (HNO_3), hydrochloric acid (HCl) were of analytical grade and purchased locally. High-purity corn stover alkaline lignin was purchased from Jinan Yang Hai Environmental Protection Material Co., Ltd (Shandong, China). The elemental compositions of the lignin were determined to be 59.96% C, 5.48% H, 0.81% N, 0.17% S and 33.58% O. The LFFC fixture used for discharging test was provided by Wuhan Zhisheng New Energy Co., Ltd. (Wuhan, China). Nafion®115 proton exchange membrane was use as the separator. High-purity Ni foam was purchased from Kunshan Shengshi Jingxin New Material Co., Ltd.

2.2. Synthesis and characterization of CoS modified anode

CoS@Ni foam electrodes was prepared via a simple electrochemical deposition technique at 25 °C. Briefly, the experiment was performed on an CHI760e Electrochemical Workstation (Shanghai Chenhua Instrument Co., Ltd, Shanghai, China) with a three-electrode configuration consisting of a Pt net (1 cm^2 ×1 cm^2) counter electrode, an Ag/AgCl reference electrode and a working electrode. Ni foam was used as the working electrode. Prior to electrochemical deposition, Ni foam was cut into pieces of 2 cm^2 × 3 cm^2 and ultrasonically washed by concentrated HCl, anhydrous ethanol and DI water successively. The Ni foam was then dried in an oven at 60 °C for 1 h. 0.05 mol/L $CoCl_2$ and 0.5 mol/L CH_4N_2S were mixed to prepare the electrodeposition solution. The CoS@Ni foam electrode was prepared by chronoamperometry technique at a constant voltage of − 1 V vs Ag/AgCl for 30 min. The prepared CoS@Ni foam electrode was washed by DI water and dried at 60 °C for 1 h. Other metal sulfide@Ni foam electrodes were prepared under the same conditions.

A scanning electron microscope (SEM) equipped with an energy dispersive X-ray spectrometer (EDS) (Hitachi S-3400 N II, Hitachi, Japan) was used to study the morphology and composition of the CoS@Ni foam. X-ray diffraction (XRD) was conducted in a D/Max 2500 H (Rigaku, Japan) diffractometer to analyze the change of crystallographic structure of the anode. The elemental chemical states of the anode catalysts were characterized by X-ray photoelectron spectroscopy (XPS) by a Thermo Fisher ESCALAB 250 Xi X-ray photoelectron spectrometer (Thermo Fisher, MA, USA).

2.3. Electrochemical measurements

Cyclic voltammetry test (CV), electrochemical impedance spectroscopy (EIS) and constant-potential electrolysis test were performed in a typical three-electrodes systems with the prepared electrode as the working electrode, Ag/AgCl electrode as a reference electrode and Pt net as a counter electrode. The electrochemical measurement was conducted in KOH solution with or without lignin. The cyclic reversibility of the prepared electrode was investigated using CV test with a scan rate between 10 mV/s and 50 mV/s. EIS test was also recorded under constant voltage of 0.45 V vs Ag/AgCl with an AC turbulence voltage amplitude of 5 mV in the frequency range of 100 kHz to 0.01 Hz.

2.4. Assembly of the liquid flow fuel cell and discharging performance measurement

The LFFC device used in the experiments was composed of two bipolar graphite plates as anode and cathode. A copper plate was fit tightly on each of the graphite plate to collect the current. A square flow chamber was carved on the middle of each graphite plates in 1 cm width× 1 cm length× 0.2 cm depth. For the anode side, the prepared CoS@Ni foam was cut into pieces of 1 cm × 1 cm and filled in the anode chamber. Hence, the electrode could be immersed by the electrolyte. A carbon foam was filled in the chamber of the cathode graphite plates. A Nafion®115 proton exchange membrane was sandwiched between the two graphite plates to separate the anolyte and catholyte and to ensure the transportation of cation ions (K^+). Two containers filled with anolyte and catholyte which were termed as anode and cathode reactors, respectively, were connected to the flow chambers by silicone tubes. Peristaltic pumps were used to pump the electrolyte into the flow champers and then back to the reactors. To investigate the effect of discharging temperature, graphite plates were heated to the test temperature using electric heating rods.

In this work, $(VO_2)_2SO_4$ (vanadyl(V) sulfate) was used as the cathode electron mediator to receive electrons and transfer them to O_2, the final electron acceptor. $(VO_2)_2SO_4$ solution was prepared according to the early reported procedure [17]. The concentration of $(VO_2)_2SO_4$ was 0.37 mol/L. Our previous studies [3,11] have shown that $VOSO_4$ (vanadyl(IV) sulfate), the reduction state, could be oxidized to $(VO_2)_2SO_4$ under the catalysis of HNO_3. An airtight internal recycle reactor composed of a three-neck flask connecting with a condenser and an air bag and a peristaltic pump was used to increase the oxidation rate of $VOSO_4$. This design could reduce the leakage of gas intermediates including NO and NO_2. In the long-term discharging test, the volume of catholyte was 300 ml, while 50 ml anolyte was used.

The polarization curve of the LFFC was obtained through the linear sweep voltammetry (LSV) from zero voltage to the open-circuit voltage at a voltage scan rate of 5–10 mV/s. LSV test is a commonly used electrochemical method to determine the polar curves and peak power density curves of different kinds of fuel cell and battery technologies

such as PEMFC, Zn-air battery and redox flow cells [18,19]. The scan rate of LSV test is usually below than 10 mV/s to ensure the determination accuracy of fuel cell performance [19]. The long-term discharging performance of the LFFC was conducted using chronoamperometry at a constant discharging voltage of 0.6 V. The anodic Faraday efficiency ($\varepsilon_{\text{anode}}$) was defined based on the following equation to describe the efficiency of electron transfer from lignin to the LFFC:

$$\varepsilon_{\text{anode}} = \frac{Q_{circuit}}{Q_{\text{anode}}} = \frac{\int It}{Q_{\text{anode}}} \tag{1}$$

where Q_{circuit} is the quantity of electrons passing through the external circuit, and Q_{anode} is the quantity of electrons transferred from lignin. Q_{anode} could be measured from the chemical oxygen demand (COD) change of anolyte containing lignin based on the following equation.

$$Q_{anode} = \frac{n_{O_2} \times (\text{COD}_0 - \text{COD}_t) \times F \times V}{1000 \times M_{O_2}} \tag{2}$$

where $n_{O_2} = 4$, is the number of electrons transferred when one molecule of oxygen is reduced to water; COD_0 (mg/L) and COD_t are the initial COD of anolyte and COD of the anolyte after discharging for t hours, respectively; F is faraday constant with value of 96485 C/mol; V (ml) is the volume of anolyte; and M_{O_2} is the molar mass of oxygen (32 g/mol). The increase efficiency of peak power density (η_P) was defined based on the follow equation:

$$\eta_P = \frac{P_{\text{max ,with lignin}} - P_{\text{max ,without lignin}}}{P_{\text{max ,without lignin}}} \tag{3}$$

which reflects the degree of power density increase after fueling lignin. The energy efficiency (η_E) of lignin-to-electricity conversion is defined as the ratio between electrical energy output by the LFFC and the energy value (higher heating value) of initial lignin fed into the LFFC :

$$\eta_E = \frac{E_{\text{electrical energy}}}{E_{lignin}} = \frac{UQ}{m_0 q} \tag{4}$$

where U is the output voltage during the long-term discharging tests; Q is the quantity of transferred electrons; m_0 is the initial mass of lignin used for discharging; and q is the energy value of lignin (24 MJ/kg).

2.5. Characterization of lignin

Some modern instrumental analysis methods were used to analyze the degradation products and structural changes of lignin before and after discharging, mainly including UV–vis spectra, FT-IR spectra, 2D-HSQC NMR spectra, GC-MS and GPC. Since lignin was insoluble in acid solution, the solid residues of lignin after long-term discharging were precipitated after acidifying the anolyte using concentrated HCl.

$$\text{lignin} - \text{H}n + \frac{n}{4}\text{O}_2 + n\text{H}^+ + n\text{OH}^- \longrightarrow^{\text{electrocatalystsandelectronmediators}} \text{Oxidized products} + \frac{3n}{2}\text{H}_2\text{O} \tag{9}$$

After filtration, the acidified anolyte was further extracted with ethyl acetate for several times to obtain small-molecule degradation products.

The UV–vis spectra were recorded with a Shimadzu UV-1800 spectrophotometer. The FT-IR spectra were recorded with a Thermo Scientific Nicolet iN10 FTIR Microscope (Thermo Nicolet Corporation, Madison, WI, USA). KBr pellets embedded with acetone-dried were made with sample concentration of about 1 mg/100 mg KBr. 2D-HSQC NMR spectra of lignin were conducted using a Bruker Advance III 400 MHz spectrometer at room temperature (~25 °C). About 30 mg sample was dissolved in 30 ml DMSO-d6 solvent. The spectral widths were 5000 and 18000 Hz for the 1 H and ^{13}C dimensions, respectively. The number of collected complex points was 1024 for the ^{1}H dimension and 256 for the ^{13}C dimension with a recycle delay of 1.5 s and several transients of 32. The small molecular degradation products of lignin were further analyzed using GC-MS systems equipped with an Agilent 7820 A, an Agilent 5975 mass-selective detector (EI at 70 eV) and a 30 m × 0.25 mm × 0.25 μm DB-5MS capillary column (Agilent Technologies, Inc., Santa Clara, CA). The oven was heated from 50 ℃ to 280 ℃ at a heating rate of 5 ℃/min. The chemical structures of the degradation products were obtained by comparison with the standard mass spectrometry in the NIST database. The average molecular weight change of lignin before and after discharging was analyzed with a Gel permeation chromatography (GPC) system (SHIMADZU GPC-8026 column and an SPD-20A UV detector). The total phenolic hydroxyl group (Ph-OH) content of lignin was determined using Folin-Ciocalteu method [20,21]. Standard curve was prepared with vanillin as the substrate at the absorbance of 760 nm, which was the characteristic absorption wavelength of reduced phosphomolybdic acid).

3. Results and discussion

3.1. Design of the liquid flow fuel cell with solid anodic electrocatalysts

The working principle of LFFC equipped with a solid electrocatalysts-loaded anode and VO_2^+/VO^{2+} as the cathode electron mediators is illustrated in Fig. 1A. The reactions taking place in different parts of the LFFCs are described as follows:

In the anode discharging chamber, lignin is oxidized to form oxidized products under the catalysis of the solid electrocatalysts in alkaline medium:

$$\text{lignin} - \text{H}_n + n\text{OH}^- \longrightarrow^{\text{electrocatalysts}} \text{Oxidized products} + n\text{H}_2\text{O} + ne^- \tag{5}$$

In the cathode discharging chamber, VO_2^+ obtains electrons from external circuit and is reduced to VO^{2+}. Electricity is thus generated because of the directional migration of electrons driven by the electrode potential difference.

$$VO_2^+ + e^- + 2\text{H}^+ \rightarrow VO^{2+} + \text{H}_2\text{O} \tag{6}$$

In the cathode reactor, the reduction form of cathodic electron mediator, VO^{2+} is oxidized by O_2, the final electron acceptor, under the catalysis of nitric acid to regenerate VO_2^+.

$$4VO^{2+} + \text{O}_2 + 2\text{H}_2\text{O} \longrightarrow^{\text{HNO}_3} 4VO_2^+ + 4\text{H}^+ \tag{7}$$

Therefore, the net cathodic reaction is the reduction of oxygen:

$$\text{O}_2 + 4e^- + 4\text{H}^+ \rightarrow 2\text{H}_2\text{O} \tag{8}$$

The overall reaction can be simply described as:

Based on the Nernst equation, the theoretical voltage of this lignin-fueled LFFC can be calculated by the following equation:

$$E_{cell} = E^{\theta}_{cathode} - E^{\theta}_{anode} + \frac{RT}{F}\left(\ln\frac{\alpha_{VO_2^+} \times \alpha^2_{H^+}}{\alpha_{VO^{2+}}} + \frac{1}{n}\ln\frac{\alpha_{lignin} \times (\alpha_{OH^-})^n}{\alpha_{oxidized\ products}}\right) \tag{10}$$

where α represents the activity of active species directly participating in the electrode reactions.

The solid electrocatalysts should have oxidizing ability in order to

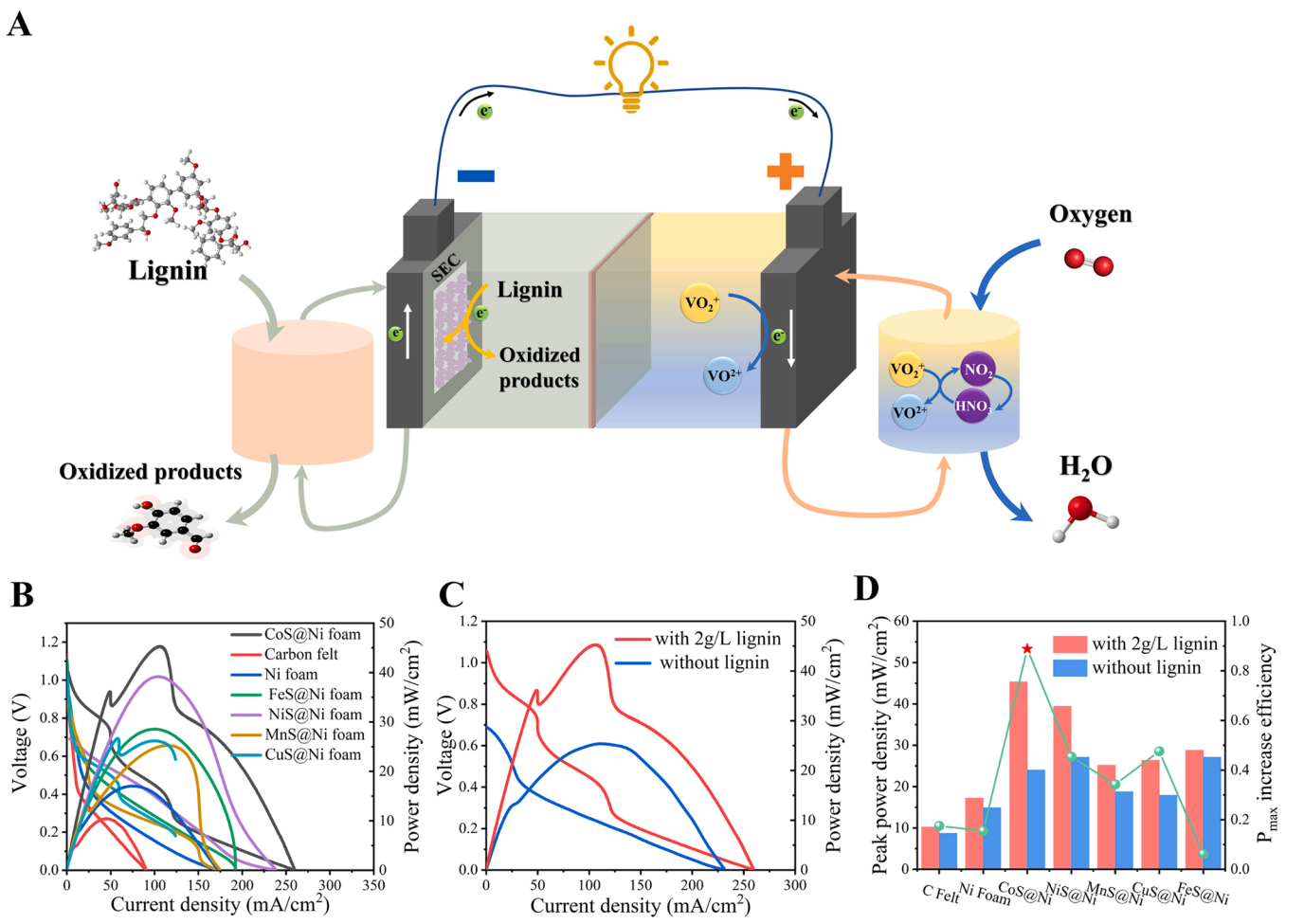

Fig. 1. Principle and screening of solid anodic catalysts for the lignin-fueled LFFC. (A): the working principle of LFFC equipped with solid anodic electron mediators modified anode and VO_2^+/VO^{2+} as the cathode electron mediators; (B): polarization curves and power density curves of LFFC with several solid anodic electron mediators in 1 M KOH with or without fueling lignin; (C): polarization curves and power density curves of LFFC with CoS@Ni anode as a solid anodic electron mediator in 1 M KOH with or without fueling lignin; (D): comparison on the peak power density of LFFCs with several solid anodic electrocatalysts. The LFFC discharging was performed at 40 °C.

extract electrons from lignin, especially from the soluble part of lignin in the anolyte. Moreover, during the electron transfer process, both the reduction and oxidation form of the solid electrocatalysts should maintain solid state to avoid further separation procedure. Since lignin has poor solubility in acidic electrolyte, alkaline anolyte is preferred. Therefore, it is required that the anodic electrocatalysts should be stable in alkaline medium.

Recently, metal sulfide has attracted much attention as electrode materials in supercapacitors because of their unique electrochemical properties, low cost, and high stability [22,23]. Inspired by this, we prepared anodes loaded with a series of metal sulfides on Ni foam using electrodeposition methods. By using VO^{2+}/VO_2^+ redox couple as the cathodic electron mediators in 2 M H_2SO_4, a LFFC system can be constructed. This system also employs an alkaline anolyte-acidic catholyte asymmetric design, which can obtain chemical bias to increase the open circuit voltage (OCV) of the cell and improve the cell performance according to the Nernst equation [24]. As displayed in Fig. 1B, some metal sulfides were tested for their capability to catalyze oxidation of lignin. Compared with untreated carbon felt and Ni foam, the anode coated with a layer of metal sulfide indeed showed better discharging performance. Among these metal sulfides, CoS possessed the best discharging performance, followed by NiS, FeS and CuS. However, MnS showed much poorer performance. Therefore, CoS@Ni foam was successfully screened as the best anode for converting lignin to electricity by the LFFC system developed in this work.

To further confirm that lignin participated in the anodic oxidation reactions, a control experiment was performed as shown Fig. 1C. In the absence of lignin, the LFFC could generate electricity with a peak power density (P_{max}) of 24 mW/cm^2. This was because the strong oxidizing ability of VO^{2+}/VO_2^+ might oxidize OH^- in anolyte to form oxygen gas (oxygen evolution reaction, OER) thus generating electricity. Since the used anolyte was 1 mol/L KOH, the theoretical electrode potential of OER could be estimated as 0.4 V vs SHE at 1 atm and 25 °C based on the Nernst equation, which was lower than the electrode potential of VO^{2+}/VO_2^+ redox couple (1.07 V). Formation of gas was indeed observed from anode discharging chamber, confirming the generation of oxygen. However, when lignin was present in the anolyte, better discharging performance was observed. The OCV of the cell increased to 1.08 V with significant increase in P_{max} to 45 mW/cm^2, which was about 1.8 times higher than that obtained with no lignin. Such an impressive increase in the LFFC performance clearly indicated that lignin indeed participated in the anodic reaction. Similarly, increase in peak power density could be observed when LFFCs with other metal sulfide anodes were used for discharging, as illustrated in Fig. 1D. We further defined a parameter termed increase efficiency of peak power density (η_P) to describe the effect of presence of lignin on electricity generation. Among those mental sulfide electrodes, LFFC with CoS@Ni foam anode had the highest P_{max} increase efficiency (Fig. 1D), suggesting that CoS was

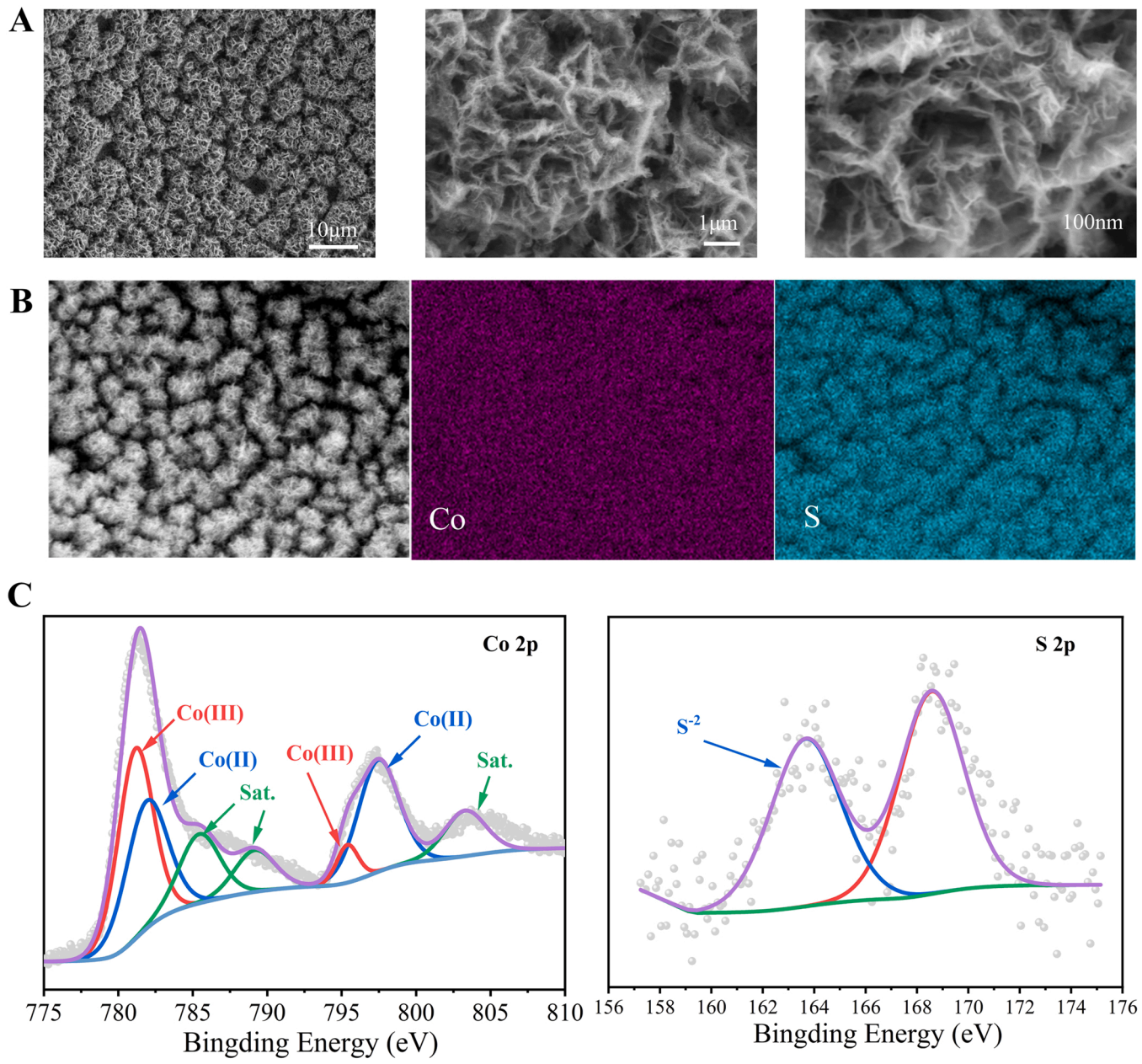

Fig. 2. Characterization of the prepared CoS@Ni foam anode. (A) SEM; (B) EDS; and (C) XPS.

indeed the best solid anodic electrocatalyst for catalyzing the oxidation of lignin on anode.

3.2. Characterization of CoS@Ni foam anode

The morphologies of the prepared anode were observed by scanning electron microscope (SEM). As shown in Fig. 2A, the CoS layer grew uniformly on the nickel foam substrate as thin nanosheets. The CoS nanosheets were generally vertically aligned on the Ni foam. The growth orientation of the CoS nanosheets was random, being overlapping and connecting with each other, thus forming a three-dimensional network structure. This structure could well increase the specific surface area for the anodic reactions. Energy-dispersive spectroscopy (EDS) elemental mapping images were further recorded to analyze the distribution of CoS species. As shown in Fig. 2B, the EDS images clearly confirmed the presence of Co and S in the nanosheets. The Co and S mapping images were well consistent with the original SEM images, indicating that Co and S species were uniformly distributed on the nanosheets.

X-ray photoelectron spectroscopy (XPS) were further performed to investigate the electronic structure of CoS nanosheet surface, as shown in Fig. 2C. The high-resolution spectrum of Co2p displayed two spin-orbit doublets with a binding range from 775 to 810 eV. The deconvolution of Co2p indicated CoS@Ni anode had pin–orbit doublets at 780.2 eV and 795.5 eV corresponding to the Co (III), and those peaks at 782.1 eV and 797.5 eV corresponding to the Co(II) [25]. Moreover, many excitation satellite peaks can also be captured, which were ascribed to the configuration of $2d^5 3d^7$ (ground state of Co(II)) and $2d^5 3d^8 L$ of Co species[26]. Moreover, for the S2p XPS high-resolution spectrum, a doublet locating at 163.7 eV and 168.7 eV could be observed. Especially, the peak at 163.7 eV are attributed to the presence of S^{2-} in the CoS@Ni foam anode. In summary, the XPS results were well consist with EDS mapping images indicating that Co(II), Co(III) and S^{2-} species were coexisting in the CoS nanosheets. The crystal structure of CoS@Ni anode was analyzed by XRD as illustrated in Supporting Information Fig. S1. The XRD pattern of CoS@Ni anode displayed three sharp peaks at $2\theta = 44.48$, $2\theta = 51.83$, $2\theta = 76.35$, respectively,which

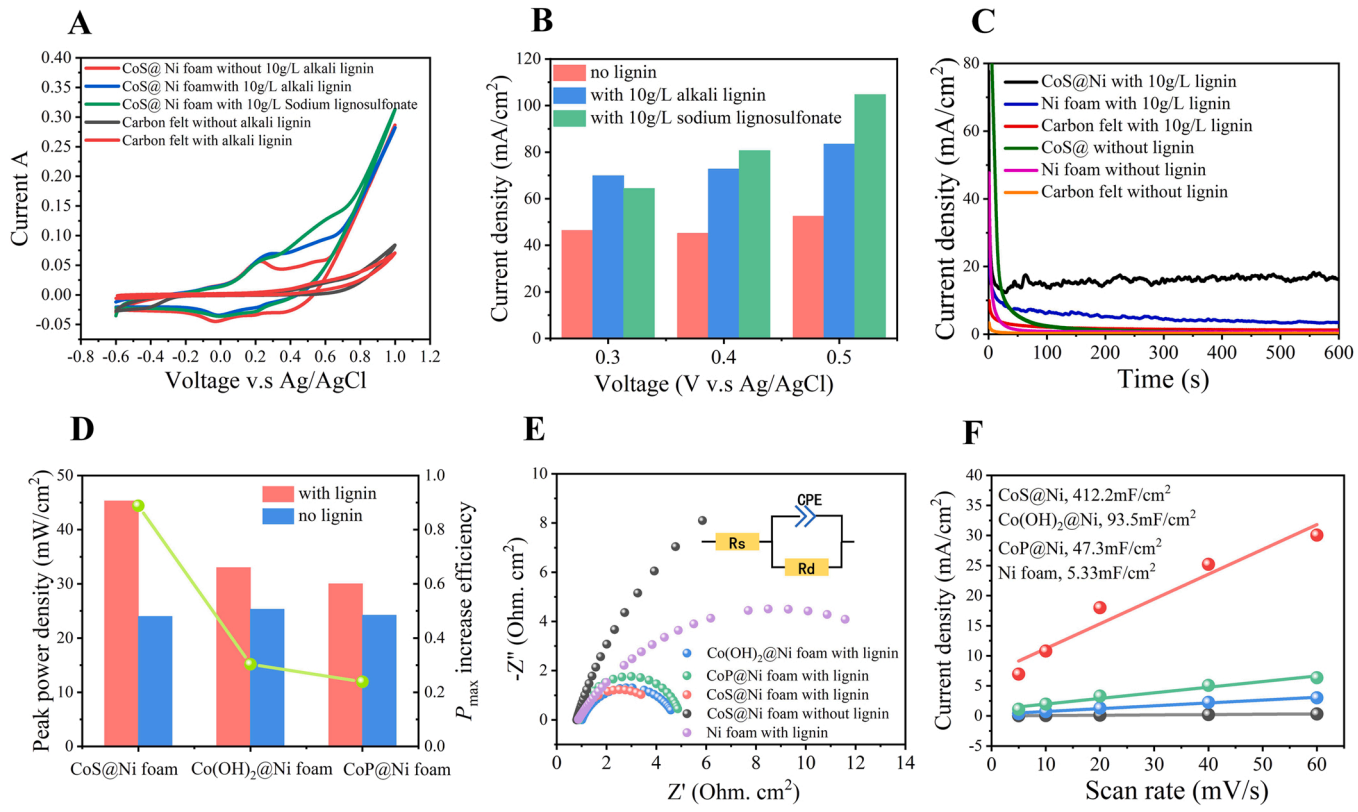

Fig. 3. Electrochemical tests of cobalt-based catalysts for converting lignin to electricity with vanadyl(V) sulfate as the cathodic electron carrier. (A): CV curves of CoS@Ni foam anode in 1 M KOH solution with or without lignin; (B): anodic current density of CoS@Ni foam at different electrode potential with or without lignin; (C): current density v.s. time of CoS electrode with or without lignin at constant 0.4 V v.s Ag/AgCl; D: comparison on the power density of LFFCs with different Co-based electrocatalysts in 1 M KOH with or without lignin; (E): EIS curves at constant 0.4 V v.s Ag/AgCl in 1 M KOH; and (F): current density as a function of scan rates for different Co@Ni electrodes.

were ascribed to the (111), (020) and (022) planes of Ni phase[27]. No other peaks corresponding to the CoS crystal could be found, indicating that the as-prepared CoS catalyst primarily existed as amorphous form.

The electrochemical properties of CoS@Ni anode were further analyzed. Fig. 3A presents the cyclic voltammetry curves of CoS@Ni anode with or without presence of lignin in 1 M KOH electrolyte. The CoS@Ni anode showed a pair of quasi-reversible redox peaks ascribed to Co^{2+}/Co^{3+} redox couples in the absence of lignin. Moreover, the electrode also showed an OER performance when the applied voltage was larger than 0.6 V v.s Ag/AgCl. In the absence of lignin, as shown in Fig. S2 the plots of anodic peak current (i_{pa}) and cathodic peak current (i_{pc}) over the square root of scan rate($v^{1/2}$) showed good linear relation, indicating that those electrochemical reactions were controlled by the diffusion of active species (OH^-) rather than the electron transportation of oxidation reaction. After adding lignin into the electrolyte, an evident increase in anodic peak current could be observed (Fig. 3B), suggesting that the electrochemically generated Co^{3+} participated in the oxidation of lignin. However, since the lignin was dissolved in the alkaline electrolyte, direct oxidation of lignin on the anode, namely the intrinsic electrochemical oxidation of lignin might also take place. In order to further confirm whether the increase in the CV oxidation peak current after addition of lignin was caused by CoS-catalyzed oxidation of lignin, CV curves of lignin fuel under the same conditions with fresh carbon felt as electrode was recorded as displayed in Fig. 3A. Since no electrocatalysts were loaded on the carbon felt, the obtained CV curve could efficiently reflect the intrinsic electrochemical behavior of lignin oxidation. It should be noted that we did not use Ni foam as a working electrode, because the $Ni^{2+/3+}$ species formed during the CV test might interfere with the determination results of electrochemical behavior of lignin. As shown in Fig. 3A, a very slight current improvement can be observed in the current range of 0.3–0.8 V v.s Ag/AgCl, which might be caused by the electro-oxidation of phenol structures in lignin. For CoS@Ni foam electrode, much higher increment on the current was observed when lignin was present, and in contrast the increment of the current for carbon felt electrode actually could be neglected. This result clearly indicated that the increase in the oxidation current in CV test was due to the oxidation of lignin by the electrocatalyst rather than the intrinsic electrochemical behavior of lignin (direct oxidation on the electrode).

Fig. 3B also shows that the anodic currents were increased by at least 25 mA/cm^2 at voltage of 0.3, 0.4 and 0.5 V v.s Ag/AgCl. Compared to the alkali lignin, using sodium lignosulfonate as the fuel resulted in more obvious increase in the current density, suggesting that sodium lignosulfonate was more likely to oxidize. To further verify the activity of electrochemical generated Co^{3+} on lignin oxidation, a relative long-term electrolysis test at constant 0.4 V v.s Ag/AgCl in a typical three electrode systems was conducted, as shown in Fig. 3C. According to the CV result, OER would not occur at voltage of 0.4 V; therefore, the current detected in the electrolysis process in the absence of lignin was primarily caused by the oxidation of Co^{2+} species to Co^{3+}. The electrolytic current dropped sharply to near zero during the 600 s of electrolysis, demonstrating the rapid depletion of reduced Co^{3+} species. With addition of lignin, the electrolytic current rapidly decreased within the initial 20 s and then stabilized at about 16 mA/cm^2, suggesting that the newly formed Co^{3+} species were chemically reduced to Co^{2+} by lignin and the reduced Co^{2+} was then electrochemically oxidized to Co^{3+} species. However, when carbon felt without loading of CoS was used as the electrode, the detected current density was very low for both cases of with or without lignin. Ni foam without loading of CoS was also used for electrolysis of lignin for comparison. The obtained current density was

higher than that obtained with carbon felt; however, the current density was still much lower than that obtained by using CoS@Ni foam electrode. Moreover, the electrode potential of CoS@Ni anode was depended on the changes of Co^{2+} and Co^{3+} species [28]. The open-circuit potential versus time (OCP-t) was further recorded to decouple the chemical reduction of Co^{3+} and electrochemical oxidation of Co^{2+} to verify the electron transfer mediated by Co^{2+}/Co^{3+}. Before test, a constant voltage of 0.4 V v.s Ag/AgCl was applied to the CoS@Ni electrode until the electrolytic current tended to be 0, which indicated that Co^{2+} species were fully oxidized to Co^{3+}. Then, the OPC-t curves was recorded immediately. As shown in Fig. S3 in Supporting Information, in 1 M KOH solution, the electrode potential of CoS@Ni electrode decreased slowly from 0.4 V v.s Ag/AgCl to 0.3 V v.s Ag/AgCl, which might be caused by the reduction of Co^{3+} by OH^-. However, addition of lignin significantly accelerated the reduction of Co^{3+}. The electrode potential of CoS@Ni electrode decreased rapidly from 0.4 V v.s Ag/AgCl to − 0.15 V v.s Ag/AgCl within 2400 s. This accelerated quenching further confirmed that the electrochemically generated Co^{3+} was the active species in lignin oxidation. Therefore, these results clearly indicated the efficiency of CoS as an electrocatalyst to catalyze the electrochemical oxidation of lignin.

We further investigated the influence of complex anions of the cobalt salts. CoP@Ni and $Co(OH)_2$ @Ni electrodes were prepared with electrodeposition at constant votage of − 1 V v.s Ag/AgCl being just like that used for CoS@Ni electrodes. SEM images and EDX elemental mapping images confirmed that CoP and $Co(OH)_2$ layers were successfully deposited on the framework of Ni foam (Fig. S4 and S5). The discharging performances of LFFCs with CoP@Ni and $Co(OH)_2$ @Ni anodes were further investigated. As displayed in Fig. 3D, the LFFCs with CoP@Ni and $Co(OH)_2$ @Ni anodes showed somewhat poorer power density than that with CoS@Ni anode. To further compare the electron transfer kinetics at the electrode-electrolyte interface, electrochemical impedance spectroscopy (EIS) test was conducted. As shown in Fig. 3E, a typical circuit model composed of a constant phase element (CPE) and two resistances was employed to simulate the obtained EIS curves. CPE is usually used to describe the imperfect capacitor behavior caused by the depressed semicircles of the obtained EIS curves [29]. EIS test indicated that addition of lignin into the anolyte have no effect on the solution resistance (Rs) at 0.4 V v.s Ag/AgCl. However, the fitted interfacial charge transfer resistance (Rt) of CoS@Ni anode decreased from 33.27 Ω in the absence of lignin to 3.48 Ω with addition of 10 g/L lignin, indicating that lignin was oxidized to accelerate the electron transfer in the anodic reaction. Furthermore, it was also found that the Rt of CoS@Ni foam was much smaller than that of Ni foam (15.90 Ω) in anolyte containing lignin, demonstrating that CoS had much higher electron transfer rate. The Rt of $Co(OH)_2$ @Ni and CoP@Ni anodes was also larger than that of CoS@Ni anode. Besides the introduction of active sites with high catalyst activity, the electrochemically active surface area is another important aspect for the electrocatalytic activity. As displayed in Fig. S6 and Fig. 3 F, the double-layer capacitance (Cdl) of the electrodes were obtained from current density-CV voltage scan rate curves. Cdl of the prepared CoS@Ni foam electrode was 412.2 mF/cm^2, which was about 75 times higher than that of the pure Ni foam (5.33 mF/cm^2), suggesting that the electrodeposition of CoS layer greatly increased the surface roughness and provided more electrochemical active sites for lignin oxidation [29]. Moreover, the Cdl of CoS@Ni was also larger than CoP@Ni and $Co(OH)_2$ @Ni, further demonstrating that better discharging performance could be obtained for the electrode with higher Cdl. Therefore, the above electrochemical analysis results clearly demonstrated that the prepared CoS@Ni anode could efficiently promote the electron transfer from lignin to electrode thus generating electricity.

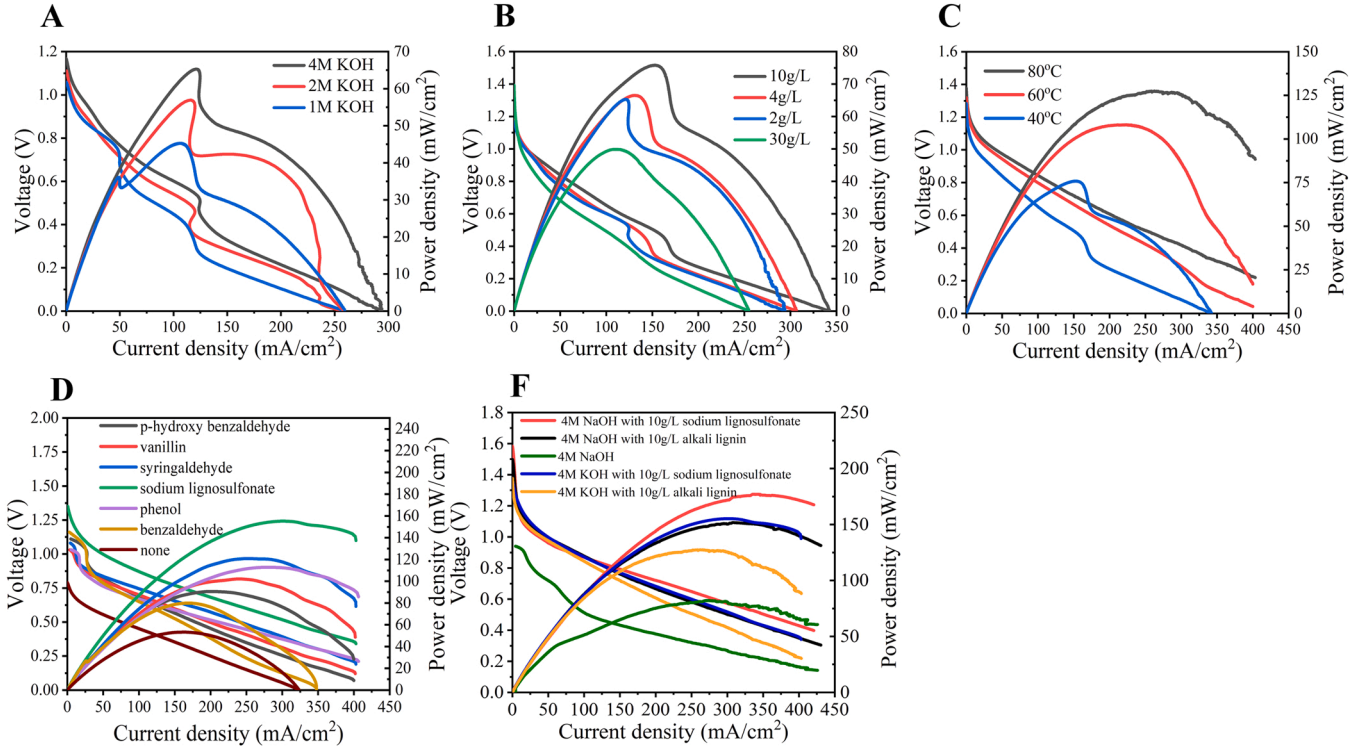

Fig. 4. Effects of operational parameters on the discharging performance of the LFFC with CoS@Ni anode. (A): effect of KOH concentration. The discharging was operated at 40 ℃ with 2 g/L alkali lignin; (B): effect of alkali lignin concentration. The discharging was operated at 40 ℃ with 4 M KOH as anolyte; (C): effect of discharging temperature. The anolyte consisted of 4 M KOH and 10 g/L alkali lignin; (D): conversion of different organic fuels for electricity generation by the LFFC developed in this work at 80 ℃; and (E) comparison on the discharging performance using NaOH and KOH as supporting anolyte at 80 °C with 2 M H_2SO_4 and 0.37 M $(VO_2)_2SO_4$ as catholyte.

3.3. Effects of operational parameters on the discharging performance of the LFFCs

Some operational parameters including KOH concentration in anolyte, lignin concentration and discharging temperature were investigated and optimized in order to obtain a higher power density, as illustrated in Fig. 4A-C. Higher peak power density could be obtained at higher KOH concentration (Fig. 4 A). Based on the Nernst equation, increasing the KOH concentration could greatly increase the chemical bias and thus obtain higher thermodynamic driving force. The inner resistance can be also reduced at high KOH concentration. Moreover, at higher alkali concentration, lignin is more likely to depolymerize, resulting in the formation of more phenolic hydroxyl group, aldehyde group and other functional groups which are more likely to oxidize [30]. Nevertheless, it should be noted that OER might became more severe as the increase in the KOH concentration resulting in the decrease in the anodic current efficiency. Lignin concentration in anolyte also affected the discharging performance. The peak power density of the LFFC increased from 65 to 75 mW/cm^2 as the lignin concentration increased from 2 to 10 g/L (Fig. 4B). This was probably because more electrons could be transferred at higher lignin concentration. However, as the lignin concentration further increased to 30 g/L, significant decrease in power density and short-circuit current density were observed. It was speculated that excessive lignin in anolyte increased the viscosity of the electrolyte, thus increasing the internal resistance and mass transfer resistance of the LFFC. Temperature had significant effect on the discharging performance as displayed in Fig. 4 C. The P_{max} of LFFC was 75 mW/cm^2 at 40 ℃ and significantly increased to 125 mW/cm^2 at 80 ℃.

Some biomass-based fuels, including sodium lignosulfonate and some lignin degradation products such as phenol, benzaldehyde, *p*-hydroxy benzaldehyde, vanillin, and syringaldehyde were used as fuels under the above optimal condition, as shown in Fig. 4D. In the absence of fuel, the P_{max} was only 55 mW/cm^2. In this case, OER took place on the anode side due to the oxidation of OH^- and water. When fuel was added, significant improvements of P_{max} were observed. The highest P_{max} of about 160 mW/cm^2 was achieved with sodium lignosulfonate as the fuel, followed by syringaldehyde, phenol, vanillin, *p*-hydroxybenzaldehyde and benzaldehyde. Compared with benzaldehydes, phenol fuels showed a higher P_{max}. This was probably because phenol hydroxyl group was more easily to oxidize than aldehyde group on CoS@Ni anode. For the three monomer aldehydes of lignin, the peak power density of the LFFC increased with the increase in the number of methoxyl group, suggesting that methoxyl group might promote the oxidation kinetics of the fuel to some extent. Moreover, compared with alkali lignin, sodium lignosulfonate had better discharging performance, which might be due to the introduction of sodium ions to increase the conductivity of the electrolyte. The effects of type of alkali including KOH and NaOH on discharging of the LFFC with sodium lignosulfonate as the fuel was further investigated, as shown in Fig. 4E. No significant difference was observed between these two alkaline anolyte for discharging at 5 g/L lignin concentration; however, the highest P_{max} of 176 mW/cm^2 was obtained with 4 M NaOH and 10 g/L sodium lignosulfonate. It indicated that the waste water discharged from alkaline pulping mills could be directly used as fuel for electricity generation. There are many types of technical lignins obtained by different industrial pretreatments or pulping of lignocellulosic biomass, mainly including the kraft, lignosulfonate, soda, hydrolyzed, organosolv lignins, among which the annual yield of kraft lignin accounts for about 80% of the total yield of different lignin [31]. Most of the technical lignins are alkaline-soluble, indicating that they can be used as fuels for the LFFC developed in this work. However, for alkaline-insoluble fuels, since solid electrocatalysts were employed to facilitate the oxidation of lignin on anode, the reaction rate would be dramatically reduced due to the poor contact between the insoluble lignin and the electrocatalysts. In this case, LFFC systems with soluble anodic electron carriers such as polyoxometalates, $Fe^{2+/3+}$ or $Fe(CN)_6^{3-/4-}$ maybe a better choice, as reported in our future work [11]. However, separation and reuse the electron carriers could be problematic. Another solution for converting alkaline-insoluble lignin to electricity with the LFFC system developed in this work is to employ solvents such as organic, ionic liquid, and deep eutectic solvents to dissolve the lignin. However, the fuel cell performance would be reduced due to the poor conductivity of the solvents. In this work, we focused on solid electrocatalysts (electron carriers) which is much easier for separation and recovery compared with liquid electron mediators. Moreover, such a LFFC may directly utilize the alkaline waste water discharged from alkaline pulping processes including the kraft, sulfite and soda processes that cover the most commonly used industrial pulping technologies for electricity generation,

Reported works on conversion of lignin to electricity by fuel cell technology is scarce. A comparison on the power density and operating conditions of some reported fuel cells for lignin-to-electricity conversion is summarized in Table 1. Microbial fuel cells (MFCs) can be operated under mild condition (room temperature); however, the power density is very low, making it be far away from practical application for power generation. Solid oxide fuel cell (SOFC) and direct carbon fuel cell (DCFC) can obtain relatively high power density. However, external processing such as gasification and pyrolysis are needed to convert lignin to suitable fuels such as CO and biochar. Moreover, SOFC and DCFC are usually operated at high temperature. LFFC mediated with liquid electron mediators have attracted more and more interest in recent years for direct conversion of biomass to electricity. However, most of the reported works employed sugars or polysaccharides as the fuels, while works on direct using lignin are scarce. In our previous works, we obtained power density of 5–200 mW/cm^2 by screening liquid electron mediators [8], but separation of the lignin degradation products and the electron mediators are challenging. In this work, by developing solid electrocatalyst modified anode, the peak power density could reach 176 mW/cm^2 with sodium lignosulfonate as the fuel, which also avoided the problem of separation of electron mediators. It seems that such a LFFC is more promising for practical application in electricity generation from organic waste such as lignin.

3.4. Electricity generation in a relatively long-term operation

To further analyze the operation stability of the LFFC for electricity generation and the structure change of lignin, a relative long-term discharging operation was conducted with nitric acid as a catalyst to catalyze the regeneration of VO_2^+ by air in an internal recycle reactor as developed in our previous work [11]. Relatively long-term discharging of the developed LFFC with 4 g/L initial lignin concentration is shown in Fig. 5A. The current density decreased from about 300 mA/cm^2 to 50 mA/cm^2 during 8-h discharging. It could be observed that the *i-t* curve of LFFC generally had two stages, which might correspond to different reaction kinetics of lignin on the anode. In the initial 30 min discharging, the current density deceased sharply. It was speculated that the original groups that were easy to oxidize including aldehyde and phenolic hydroxyl groups primarily participated in the oxidation reaction at this stage. The rapid depletion of these groups resulted in the rapid decrease in the output current density. Meanwhile, due to the strong alkalinity of the anolyte, depolymerization reaction of lignin definitely took place, exposing more functional groups with high reactivity. During the 30–120 min of discharging, a relatively stable output power density of about 150 mA/cm^2 was observed. This was because the rate of oxidation of lignin to extract electrons by Co^{3+} was similar to that of re-oxidation of Co^{2+} on the anode. As the discharging proceeded, the reactivity of residual lignin became decreased and the concentration of VO_2^+ in the cathode gradually decreased, leading to continuously decrease in the power density. It can be speculated that the current decrease in the initial discharge stage could be mitigated by increasing the lignin concentration. To confirm this, the effects of lignin concentration on the relatively-long term discharging was investigated as

Table 1
A comparison on power density of different fuel cells to convert lignin to electricity.

Fuel cell type	Lignin fuel used	External processing or pretreatment	Peak power density (P_{max}, mW/cm^2)	Operating temp. (°C)	Ref.
MFC	Sodium lignosulfonate	Photocatalytic degradation	0.0248	25	[44]
MFC	*Miscanths sacchariflorus*	Hydrolysates using sulfuric acid method	0.1995	25	[45]
PEMFC	Kraft lignin	Ni anode H_2O_2 used as oxidants in the cathode	1.4	25	[46]
PAFC	Cypress	Mixed with H_3PO_4	22	250	[47]
SOFC	Alkali lignin	Gasification to CO catalyzed by Fe_2O_3	450	800	[48]
SO-DCFC	Walnut shell	Pyrolysis to biochar at 700 °C	147	800	[49]
SO-DCFC	Sodium lignosulfonate	Pyrolysis to biochar at 400 °C	24	560	[50]
SO-DCFC	Raw oil palm mesocarp fiber	Pyrolysis to biochar at 500 °C	11.8	850	[51]
SO-DCFC	Rice husk	Pyrolysis to biochar at 600 °C	135	850	[52]
MHFC	Pine wood	Pyrolysis to biochar at 800 °C	76.6	400	[53]
MHFC	Pine bark pellet	Pyrolysis to biochar at 800 °C	45	450	[54]
MHFC	Sawdust	Pyrolysis to biochar at 400 °C	789	750	[55]
MHFC	Olive wood	Pyrolysis to biochar at 600 °C	105	700	[56]
LFFC with liquid electron mediator	Sodium lignosulfonate/kraft lignin	Electron extraction from lignin fuel by polyoxometalates	5	90	[42]
LFFC with liquid electron mediators	Wheat straw milled lignin	Electron extraction from lignin fuel by methylene blue	41.8	90	[8]
LFFC with liquid electron mediators	Alkali lignin	Electron extraction from lignin fuel by $K_3[Fe(CN)_6]$	200	90	[11]
LFFC with liquid electron mediators	Wheat straw	Electron extraction from lignin fuel by $FeCl_3$	100	90	[17]
LFFC with solid electrocatalysts	Corn stover alkali lignin	No external processing or pretreatment needed	125	80	This work
LFFC with solid electrocatalysts	Sodium lignosulfonate	No external processing or pretreatment needed	160	80	This work

MFC: Microbial fuel cell; PAFC: phosphoric acid fuel cell; SOFC: Solid oxide fuel cell; SO-DCFC: Solid oxide direct carbon fuel cell; MHFC: Molten hydroxide fuel cell; LFFC: Liquid flow fuel cell.

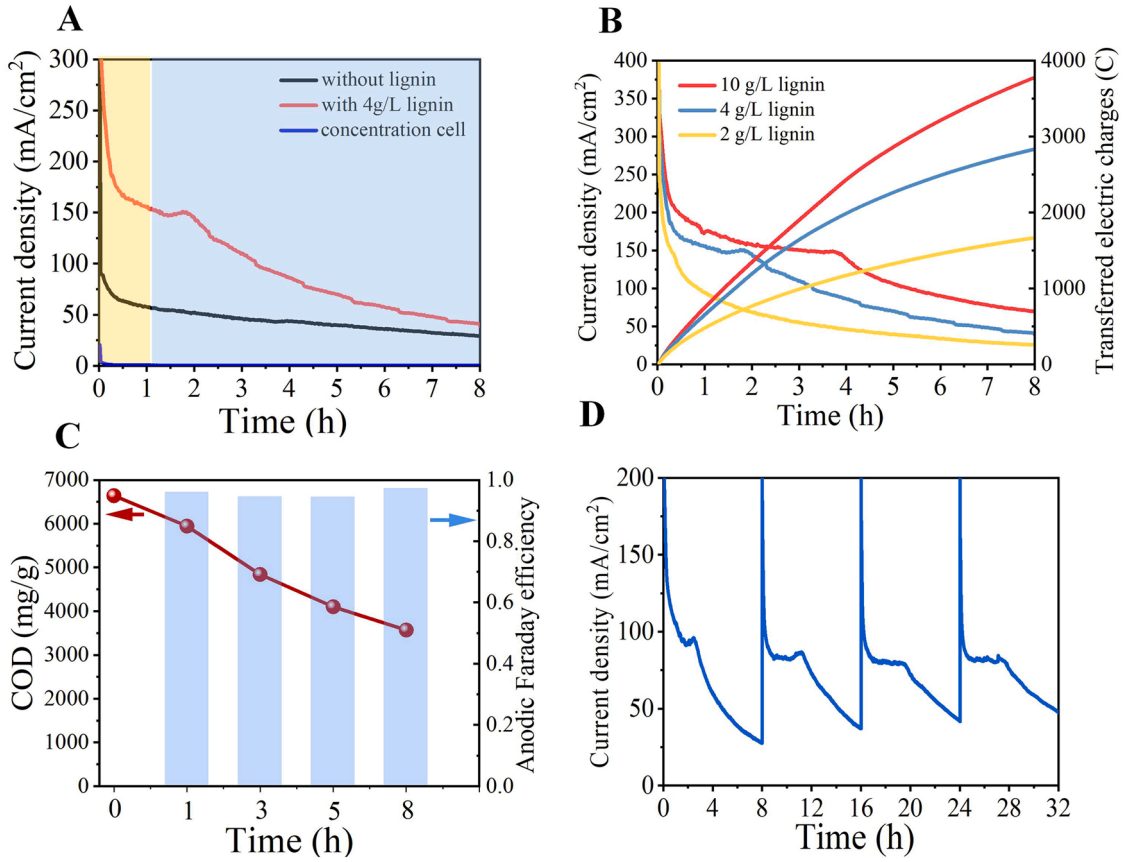

Fig. 5. Performance of the LFFC for relatively long-term discharging. (A): A relative long-term discharging at constant voltage of 0.6 V with 4 g/L initial lignin concentration; (B): effects of lignin concentration on the discharging performance; (C): COD change of anolyte and anodic Faraday efficiency during discharging of the LFFC fueled with 4 g/L lignin; and (D): output current density of the LFFC with feeding of 2 g/L lignin into anolyte every 8 h.

shown in Fig. 5B. It was clearly that more stable output current density indeed could be obtained at higher lignin concentration. For example, the current density decreased to 100 mA/cm^2 in 1 h at lignin concentration of 2 g/L, but still could be higher than 100 mA/cm^2 after 6 h at 10 g/L lignin concentration.

Furthermore, since oxygen evolution reaction might take place on the anode due to the strong oxidizing ability of the used cathode electron carriers, vanadyl(V) sulfate, it is necessary to measure the anodic efficiency excluding the contribution of water oxidation to the output current density. The anode Faraday efficiency was defined as the ratio of electron quantity received by the external circuit to that released by lignin. If the anodic Faraday efficiency is higher than 1, it would indicate that OER significantly occurred on the anode. We determined the COD change of the anolyte by potassium dichromate method which is commonly used in environmental area. Hence, the transferred electron quantity could be conveniently calculated from the COD change of the anolyte. As displayed in Fig. 5C, the COD of anolyte decreased continuously from 6640 mg O_2/L to 3561 mg O_2/L during 8-h discharging, suggesting that the lignin was indeed oxidized on the anode continuously. The anodic efficiency was estimated as 97% indicating that the OER side reaction could be neglected and the electrons transferred to the external circuit indeed was predominantly from lignin oxidation. Initial lignin concentration in the range of 2–10 g/L did not significantly affect the anodic efficiency as shown in Fig. S7. The anodic efficiency was still as high as 98% with relatively low (2 g/L) lignin concentration, indicating that the oxidation reaction of alkali lignin was predominant over OER. However, the reduction of the COD was greatly affected by the lignin concentration. COD decreased by 51.9%, 46.3% and 20.6% at initial lignin concentration of 2, 4 and 10 g/L, respectively. We further investigated the stability of LFFC system by fed-batch operation. As shown in Fig. 5D, the current density could be well recovered to 200 mA/cm^2 when lignin fuel was fed into the anolyte. After feeding for four batches for total operation time of 32 h, no significant decrease in the discharging performance was observed, indicating the stability of the CoS@Ni foam anode for mediating electron transfer.

The microstructure and electronic structure change of CoS@Ni foam anode after 32-hour discharging were further investigated. As illustrated in Fig. S8(a)-(c), the CoS nanosheet was still vertically aligned on the Ni foam being just like the freshly prepared CoS@Ni foam but the thickness of the CoS nanosheet seemed to be increased slightly. As displayed in Fig. S8(d), the EDS images further confirmed that the Co species were still spatially uniform and did not agglomerate. However, the S species disappeared while O species appeared on the surface of CoS nanosheet. The XPS results were well in accordance with EDS mapping images and indicated that the S species disappeared after 32-h of discharge. The deconvolution of Co2p suggested that both Co^{2+} species and Co^{3+} species were present on the surface of CoS nanosheet. However, compared to the fresh CoS@Ni foam electrode, the proportion of Co^{3+} seemed to be increased. For the O1s XPS high-resolution spectrum, a singlet locating at 531.20 can be observed corresponding to the $Co(OH)_2$ species or CoOOH species[32]. EDS and XPS clearly indicated that the surface of the CoS@Ni electrode was reconstructed during the discharging process which similarly was identified for many electrocatalysts [28,33,34]. It is believed that the formation of $Co(OH)_2$/CoO(OH) mixtures was caused by the OH^- ion exchange between the anode and anolyte during the discharging process. However, this ion exchange did not significantly affect the activity of the anode, because the electron transfer was majorly mediated by Co^{3+}/ Co^{2+} species.

3.5. Structure change of lignin during discharging and mechanisms of electron transfer

3.5.1. Change of lignin structure

To better understand the electron transfer efficiency, the structure change of lignin during the long-term discharging was investigated. The UV-Vis spectra of the anolyte during 8-hour discharging at constant voltage of 0.6 V was recorded as shown in Fig. S9(a) and (b). UV absorbance at 289 nm ascribed to benzene ring substituted by hydroxyl or methoxyl and at 340 nm ascribed to conjugated phenolic structures was continuously decreased, indicating that the aromatic skeleton of lignin was destroyed. To confirm that this structure change was caused by the oxidation on the anode instead of alkaline depolymerization, the LFFC was set at open-circuit condition and the UV-Vis spectra of the anolyte was similarly recorded. As illustrated in Fig. S9(b) and (c), the UV absorbance at 289 nm did not decrease apparently, while the UV absorbance at 340 nm slightly increased oppositely, suggesting formation of conjugated phenolic structures such as aromatic aldehydes or ketones [35]. This result clearly indicated that more lignin structure change indeed was caused by oxidation reactions on the anode over the CoS catalyst. The anolyte was further acidified to precipitate the residual lignin. It was found that in the control experiment with 4 M KOH treatment at 80 ℃, 99% of the original lignin could be precipitated after acidification. However, after discharging for 8 h, only about 10% of the original lignin was precipitated, suggesting that more significant depolymerization of lignin macromolecule was achieved. Moreover, gas was formed and collected during acidification of the anolyte, but no gas was formed for the control group. By using a device for anolyte acidification and gas collection shown in Fig. S10a, a total volume of 1752 ml gas was collected. GC analysis demonstrated that CO_2 was indeed detected in the gas mixture (Fig. S10b), and 5.7% of the carbon element in alkali lignin was mineralized to CO_2 during the discharging. These results further confirmed that lignin underwent deep oxidation and mineralization. Soluble lignin degradation products were further obtained by extraction with ethyl acetate and analyzed with GC-MS technique. As displayed in Fig. S11 and Table S1, diverse aliphatic acids and aromatic acids were produced by oxidation of lignin. The aliphatic acids detected included glycolic acid, malonic acid, succinic acid, and maleic acid, suggesting that benzene ring skeleton of the lignin underwent ring-opening reactions [36]. The aromatic acids including *p*-hydroxybenzoic acid, vanillic acid, and syringic acid were ascribed to the depolymerization of lignin and oxidation of side chains. However, there were still many of the degradation products being not successfully identified. For example, the oligomers of lignin monomers. Vanillin was then used as a model compound to analyze the structural changes during 8-h discharging. As displayed in Fig. S12, the degradation products included aldehyde oxidation products such as vanillic acid and *p*-hydroxybenzoic acid, *p*-benzoquinone, as the phenolic hydroxyl oxidation products, and methoxymaleic acid as a typical product resulted from benzene ring-opening reaction.

The structure of precipitated solid lignin obtained in the acidification process were further analyzed. As shown in Fig. S13a, the FT-IR spectra of precipitated lignin obtained from open-circuit condition (just treated by 4 M KOH for 8 h at 80 ℃) was almost the same as that of raw lignin. However, FT-IR spectra of precipitated lignin after 8 h discharging clearly indicated that benzene ring structure underwent damage. The intensity of band at 1591, 1505 and 1420 cm^{-1} ascribed to the aromatic skeletal vibrations became weakened significantly after discharging. Moreover, it should be noted that the oxidation degree of lignin was depended on its initial concentration. As illustrated in Fig. S13a, the FT-IR spectra change of precipitated lignin at 10 g/L initial concentration was not so obvious, but weakened intensity of band ascribed to the aromatic skeletal vibrations was observed. No precipitated lignin was obtained by acidification when the initial concentration of lignin was as low as 2 g/L. As shown in FigureS15b, with the increase in discharging time, the intensity of aromatic skeletal vibration-related bands became gradually weakened, further confirming the degradation of aromatic ring structure by the oxidation on anode. As shown in Fig. 6A, the phenolic hydroxyl content of the residual lignin decreased from 3 mmol/g of raw lignin to 0.2 mmol/g after 8-h discharging, suggesting that phenolic hydroxyl groups were involved in the oxidation reactions. Especially, the phenolic hydroxyl content decreased by about 50% within the initial 0.5-h discharging. The weight-average molecular

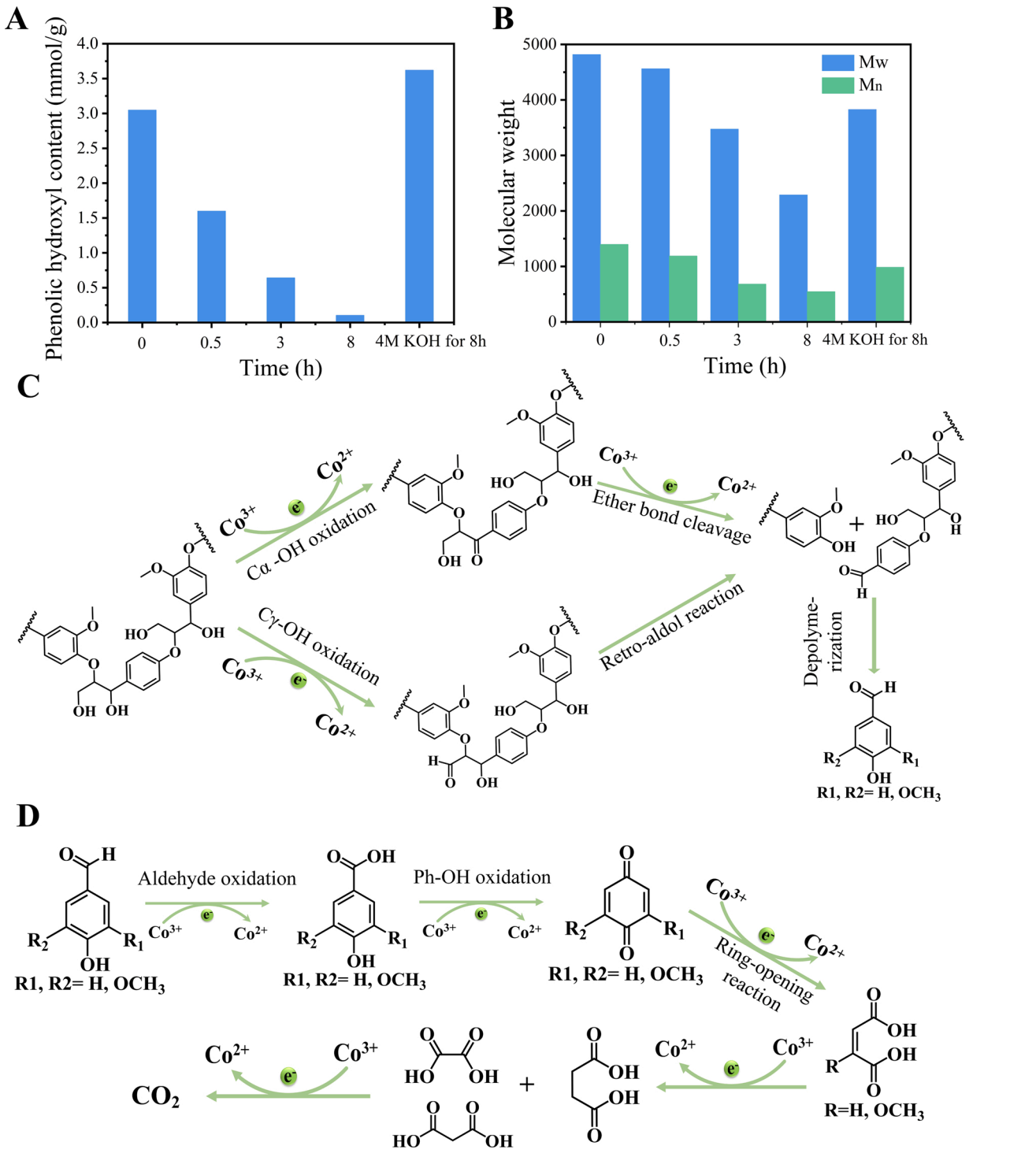

Fig. 6. Structure change of lignin during discharging. (A): phenolic hydroxyl content of precipitated lignin after discharging for different time; (B): molecular weight of precipitated lignin after discharging for different time; (C): a possible oxidation mechanism of lignin macromolecule on CoS@Ni foam anode; and (D): a possible oxidation mechanism of aromatic aldehyde monomer on CoS@Ni foam anode.

weight ($\overline{M_w}$) and number-average molecular weight ($\overline{M_n}$) decreased from 4800 and 1400 of raw alkali lignin to 2300 and 540 after 8-h discharging (Fig. 6B). It was also found that lignin underwent depolymerization to a certain degree after treatment by 4 M KOH at 80 °C, which was confirmed by the increase in phenolic hydroxyl content and somewhat decrease in molecular weight (Fig. 6A). 2D-HSQCNMR was further conducted to investigate the structure change of precipitated lignin. As displayed in Fig. S14, S15 and Table S2, raw alkali lignin showed clear signal for typical subunit structures such as syringyl units (S2,6: δC/δH 104.1/6.71), guaiacyl units (G2: δC/δH 111.2/7.29, G5: δC/δH 114.9/6.77, G6: δC/δH 119/6.50), p-hydroxybenzoate (H2,6: δC/δH 127.7/7.19), *p*-coumatate units (PCE2,6: δC/δH 130.2/7.51, PCE8: δC/δH 115.5/6.29) and ferulate units (FA2: δC/δH 110.7/7.35, FA6: δC/δH 123.8/7.20, FA7: δC/δH 114.8/7.51, FA8: δC/δH 116.9/6.39) and inter-unit linkage such as β-O-4′ aryl ether (Aα: δC/δH 71.9/4.91, Aβ: δC/δH 85.8/4.61, Aγ: δC/δH 59.9/3.35–3.8) and phenylcoumaran (β-5′, Cγ: δC/δH 62.7/3.36), respectively [11]. After discharging for 0.5 h, the signal of various chemical structure became

much weakened or even disappeared. When the discharging time increased to 8 h, much less signal was detected, suggesting the cleavage of β-O-4′ aryl ether and β-5 bonds and the destroy of aromatic units including syringyl, guaiacyl, *p*-coumatate, and ferulate units. Hence, the above results clearly demonstrated that lignin underwent significant depolymerization in LFFC during the long-term discharging process.

Based on the above results, a possible oxidation mechanism of lignin over CoS@Ni anode was proposed as shown in Fig. 6B and C. β-O-4 linkages are the most abundant linkage type in lignin macromolecule, accounting for approximately 40–65% of lignin intramolecular linkages. 2D-HSQC NMR results clearly indicated that β-O-4 linkages were significantly cleaved. As displayed in Fig. 6B, two possible reaction pathways for oxidative cleavage of β-O-4 linkages over CoS@Ni anode were thus proposed, based on the oxidation of C_α benzylic alcohol and C_γ aliphatic alcohol, respectively. Benzylic oxidation produced a ketone intermediate in C_α position which could stimulate the cleavage of ether bond mediated by Co^{3+} and result in the depolymerization of lignin [37]. On the other hand, oxidation of C_γ aliphatic alcohol led to the production of aldehyde and finally convert to phenols and aromatic aldehydes [38]. These reactions are also usually involved in chemical oxidation of lignin [39]. According to the GC-MS results, the oxidation pathway of aromatic aldehyde species formed by the depolymerization of lignin can be proposed as Fig. 6D. Oxidation of aldehyde and phenolic hydroxyl group can steadily take place to form quinone intermediates. The detection of typical benzene ring oxidation products such as maleic anhydride and methoxymaleic acid further proved that ring opening reaction of quinone intermediates occurred. Finally, the ring-opening products formed can be further degraded into small carboxylic acids and even carbon dioxide. However, due to the mild reaction condition, only a minor part of lignin was oxidized to CO_2, and most of them were present as intermediate chemicals. It has been found that the oxidation degree of lignin by electrochemical oxidation process is greatly dependent on the reaction conditions, and higher degree of oxidation usually can be achieved at higher reaction temperatures, resulting in more formation of CO_2. For instance, Hibino et al. reported a direct lignin electrolysis system operated at 150 °C for H_2 production and found that about 85% of lignin was oxidized to CO_2 in the anode [40]. Nevertheless, the obtained chemicals in this work are usually of high added-value, and they may be recovered as products for industrial application.

3.5.2. *Efficiency of the LFFC for electricity generation from lignin*

The above results clearly indicated that oxidation of lignin took place on CoS@Ni foam anode. Electrons transferred from lignin under the catalysis of Co^{3+} to vanadyl (V) (VO_2^+) and then finally to oxygen. The efficiency of the LFFC was affected by the kinetics and efficiency of both anodic and cathodic reactions for electron transfer as well as the regeneration of vanadyl (V) by air (oxygen). For long-term operation, the stability of CoS@Ni was important, and the formed vandyl (IV) (VO^{2+}) must be quickly re-oxidized to regenerate vanadyl(V)(VO_2^+). Fig. 5D showed that the current density could be well recovered after feeding lignin fuel, suggesting the good stability of the CoS as an anodic catalyst for lignin oxidation. For regeneration of cathodic electron carrier, it has been found that vanadyl (V) can be easily regenerated by air or oxygen under the catalysis of HNO_3. Our previous work on kinetics of vanadyl (IV) oxidation to form vanadyl (V) showed that 65% of vanadyl (IV) could be re-oxidized to form vanadyl(V) (re-oxidation degree of vanadyl (IV) was 65%), and thus the regenerated catholyte was a mixture of vanadyl (IV) and vanadyl (V) [3]. A relatively long-term discharging was performed with the regenerated catholyte to test the performance of the LFFC and efficiency of electron transfer. As shown in Fig. 7A, due to the oxidation degree of regenerated catholyte (~65%)

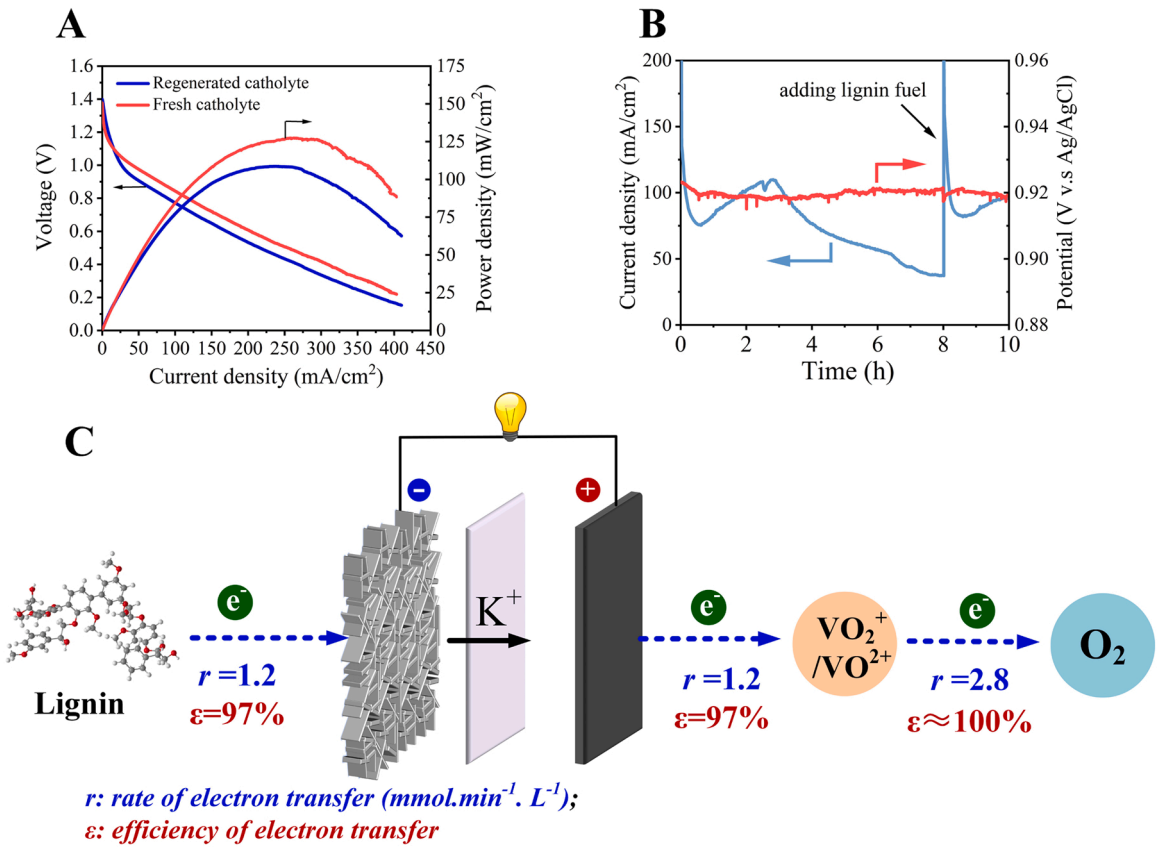

Fig. 7. Efficiency of the LFFC for converting lignin to electricity. (A): comparison on the power density of the LFFC using fresh and regenerated VO_2^+ for discharging with 2 M sulfuric acid as the supporting electrolyte; (B): current density of relatively long-term discharging and the change of cathodic potential with regenerated VO_2^+ as the cathodic electron carrier; and (C) rate and efficiency of electron transfer of the LFFC developed in this work.

was lower than the fresh catholyte (~100%), the LFFC obtained somewhat lower power density than that with fresh catholyte. However, the LFFC still could achieve a high peak power density of 110 mW/cm^2, which was still much higher than that (usually less than 50 mW/cm^2) obtained by most of the recently reported biomass-fueled LFFCs with soluble electron carriers in both the anode and cathode [2]. To investigate the stability of VO_2^+/ VO^{2+} redox couple for mediating electron transfer, an Ag/AgCl reference electrode was used to measure the catholyte electrode potential. As displayed in Fig. 7B, the LFFC exhibited similar discharging performance to that obtained by using fresh catholyte (Fig. 5A). Sharp decrease in current density could be similarly observed in the initial 30 min of discharging, suggesting that the original groups primarily participated in the oxidation reactions at this stage. During the 30–120 min of discharging, a relatively stable output power density of about 110 mA/cm^2 was observed. As the discharging proceeded, the reactivity of residual lignin became decreased, resulting in the continuously decrease in current density. Furthermore, the current density could be significantly improved by feeding fresh lignin fuel. Moreover, the electrode potential of catholyte was maintained at 0.92 V v.s Ag/AgCl during the 10-h discharging, suggesting that the VO^{2+}/VO_2^+ redox couple did act as stable electron carriers to mediate the electrons transfer from lignin to oxygen with high efficiency. This result also confirmed that VO^{2+}/VO_2^+ redox couple could quickly transfer the electrons to oxygen under the catalysis of HNO_3, while the transfer of electrons from lignin to anode seemed to be the limiting step. According to the results of relatively long-term discharging and kinetics of reoxidation of vanadyl (IV) by oxygen under the catalysis of HNO_3, the rates and efficiency of electron transfer are depicted in Fig. 7C. The anodic reaction showed an average rate of 1.2 mmol electrons min^{-1} L^{-1}, corresponding to 97% Faraday efficiency, namely that 97% of the electrons released by oxidation of lignin as determined by COD change of the anolyte could be transferred to the anode. In a quasi-steady state, the electrons released from the cathode could be completely accepted by the cathodic electron carriers, vanadyl (IV), the average rate of electron transfer was also 1.2 mmol electrons min^{-1} L^{-1} with an efficiency of 98%. The reoxidation of vanadyl (IV) to regenerate vanadyl (V) under the catalysis of HNO_3 had an electron transfer rate of 2.8 mmol electrons min^{-1} L^{-1} with about 100% efficiency, indicating that electrons could be quickly and efficiently transferred to the final oxidant, oxygen. Therefore, improving the rate of electron transfer from lignin to the anode is the key to further increasing the power density of the cell. In terms of the energy efficiency, as shown in Fig. 5B, the transferred electric charges was greatly dependent on the initial lignin concentration, while the output electric energy was also significantly dependent on the external loading. The collected transferred electrons during the discharging at a constant voltage of 0.6 V were 3783 C, 2837 C and 1669 C when the initial lignin concentrations of were 10, 4 and 2 g/L, respectively (the volume of anolyte was maintained at 50 ml). Hence, the electric energy generated could be calculated as 2270, 1702 and 1001 J, respectively. Based on the elementary compositions of alkali lignin used in this work, the higher heating value of the lignin is estimated as 22.7 kJ/g [41], it could be calculated that the energy efficiency of the LFFC developed in this work were 20.0%, 37.4% and 44.1%, respectively, based on the initial raw lignin fuel. The energy conversion efficiency of the LFFC decreased with the increase in the amount of lignin fed, which was caused by the deeper oxidation of lignin at lower lignin concentration. However, the energy efficiency of our LFFC is much higher than those of reported LFFCs fueled with biomass such as wheat straw of lignin [8]. Since lignin can be available as by-product of pulping and paper industry and lignocellulose biorefinery, it could be used as cheap fuels for electricity generation. Currently 50–70 million tons of technical lignins are produced annually by pulping and paper industries world-widely [42]. About 13,900–19,460 billion kWh of electricity can be generated from these lignins. Such a large amount of electricity is enough to power a super city like Shanghai, China, for 9–12 years (Based on the National Bureau of Statistics of Chain, the annual electricity consumption of Shanghai in 2020 is 1575.96 billion kWh). Therefore, lignin as a fuel for producing electric energy is a promoting way to reduce the dependence on fossil fuel such as coal. Nevertheless, complete oxidation of lignin was not possible by the LFFC developed in this work because the used discharging condition was much milder (80 ℃) than combustion process. Some lignin degradation products were produced as shown in Fig. 6D. These compounds are usually high value-added products and can be recovered by subsequent separation process such as extraction and adsorption.

3.5.3. Contribution of neutralization energy to electricity generation

In this work, an alkaline-acidic asymmetric anolyte and catholyte was used, which could well increase the cell voltage, namely the thermodynamic driving force for lignin oxidation, as shown by Eq. (10). Therefore, the LFFC voltage could be increased by increasing the OH^- concentration in the anolyte and the H^+ concentration in the catholyte. Generally, when a fuel cell has an "alkaline | acid" configuration, the neutralization-assisted increase in the cell voltage is 59 mV multiplied by pH difference between the cathode and anode [24]. It could be estimated that the voltage increase by using the acidic catholyte (4 M H_2SO_4) and alkaline anolyte (4 M KOH) was about 0.9 V in this work. The increase in the voltage definitely well enhanced the thermodynamic driving force of electron transfer from lignin to cathode electron carriers and finally to oxygen. Actually, acidic-alkaline asymmetry strategy has a wide range of applications in the field of fuel cells. For instance, Omar et al. [43] reported an ascorbate fuel cell with ascorbate and KOH as the anolyte while H_2O_2 and H_2SO_4 as the catholyte. The maximum power density reached 158 mW/cm^2 at 60 °C with 30% H_2O_2. Isabel et al. designed a split pH direct liquid fuel cell (DLFC) using an alkaline fuel stream containing NaOH and an alcohol fuel (glycerol, 1-propanol, or 2-propanol) with an acidic oxidant stream containing H_2SO_4 and 3% H_2O_2. The highest maximum power density for propanol DLFC with Pt black cathode reached 241 mW/cm^2. These fuel cells incorporate the advantages of both alkaline and acidic fuel cells to increase overall performance. However, it also may be concerned that neutralization might take place because of the alkaline-acidic asymmetric design. As found in our previous work [11], under the open circuit condition, OH^- concentration in anolyte as well as H^+ concentration in catholyte indeed decreased due to the crossover of H^+ from catholyte to anolyte causing neutralization. However, under the discharging conditions, because the inner electric field in the LFFC is directed from the cathode to the anode, the diffusion of H^+ from the cathode side to the anode side actually gets inhibited. Therefore, it was other cation such as K^+ instead of H^+ that diffused from anolyte to catholyte across the membrane. Nevertheless, as the discharging proceeded, we did observe that OH^- was gradually consumed on the anode side because OH^- was directly involved in the oxidation of the lignin on the anode side, and H^+ was consumed due to reduction of oxygen to form water. Hence the neutralization energy might contribute to the output electric energy. When no lignin is present in the anolyte, oxidation of OH^- to form oxygen (OER) occurs. In this case, the electrode reactions can be described as follows [24]:

Anode side:

$$4OH^- - 4e^- \rightarrow 2H_2O + O_2 \quad (11)$$

Cathode side:

$$O_2 + 4H^+ + 4e^- \rightarrow 2H_2O \quad (12)$$

The overall reaction:

$$H^+ + OH^- \rightarrow H_2O \quad (13)$$

Namely, the overall reaction is the acid-alkaline neutralization reaction, but transfer of electrons to the electrode and external circuit takes place. This process is electrochemical neutralization reaction which indeed can contribute the output electric energy. However, when

lignin is present in the anolyte, oxidation of OH^- was significantly inhibited because no bubbles were observed during discharging, and the major electrode reactions are shown as reaction (5). In this case, the consumption of OH^- is mainly caused by neutralization of the formed H^+ (organic acids or CO_2 formed by oxidation of lignin). However, using alkaline anolyte is important in this work in order to improve the kinetics of lignin oxidation and promote electron transfer. It is because lignin would gradually precipitate at anolyte pH of lower than 10, which not only reduces the rate of lignin oxidation on the anode, but also may block the pores of the electrode and cell channels leading to reduction in cell performance. To solve the problems of OH^- consumption on the anode, a possible solution is to direct use the black liquor from alkaline pulping mills which contains lignin and waste alkalis that should be treated. For small pulping mills, investment on alkali recovery system is too high, and thus the alkali is usually treated as a waste. By conversion of the black liquor to electricity, double benefits could be obtained for both energy production and waste water treatment. Likewise, the acidic environment required on the cathode side also can be maintained by supplementing industrial waste acids. More works need to be done in future for process integration and design of fuel cell devices at larger scale in order to further improve the efficiency.

However, it also should be noted that for an "alkaline | acid" asymmetric fuel cell, the cell actually cannot be operated at a true steady state. As the continuous consumption of OH^-, the cell would change to an "acid | acid" configuration. That is, the operation of an "alkaline | acid" cell finally will require a procedure to regenerate the alkaline condition of the anolyte, which requires energy. Typically, electrolysis of water can be used to regenerate the corresponding alkali and acid, which needs input energy at least equivalent to the neutralization energy. Therefore, if the output electric energy of the LFFC developed in this work is lower than the neutralization energy, the LFFC would not be energy positive. To estimate the theoretical contribution of neutralization energy to the total energy recovery, theoretical calculation was performed as follows. The elemental compositions of the lignin used in this work were determined to be 59.96% C, 5.48% H, 0.81% N, 0.17% S and 33.58% O. Therefore, the molecular formula of lignin could be simply described as $C_5H_{5.48}O_{2.1}$ by ignoring the S and N contents due to their low proportions. Hence, the related reactions of the LFFC can be described as follow:

Anode side:

$$C_5H_{5.48}O_{2.1} + 21.28OH^- - 21.28e^- \rightarrow 5CO_2 + 13.38H_2O \quad (14)$$

Cathode side:

$$5.32O_2 + 21.28H^+ + 21.28e^- \rightarrow 10.64H_2O \quad (15)$$

The overall reaction:

$$C_5H_{5.48}O_{2.1} + 21.28OH^- + 21.28H^+ + 5.32O_2 \rightarrow 5CO_2 + 24.02H_2O \quad (16)$$

Theoretically complete oxidation of 1 mol lignin to CO_2 in LFFC will consume 21.28 mol of H^+/OH^-. Based on the result of elemental analysis, the heat value of the used lignin could be estimated as 22.71 kJ/g, or 10,938.7 kJ/mol ($\overline{M_w}$=4816 g/mol as determined by GPC). It has been known that the electrochemical neutralization energy is 79.9 kJ/mol. Accordingly, 1700 kJ of electrochemical neutralization energy would be provided by the consumption of H^+ and OH^-, if OH^- oxidation simultaneously occurs on the anode. However, this neutralization energy is just 15.5% of the heating value of 1 mol lignin. Therefore, most of the electric energy produced by the LFFC developed in this work actually comes from the oxidation of lignin. Nevertheless, the energy conversion efficiency is also greatly dependent on the degree of oxidation of lignin.

Moreover, an important issue that should be considered is whether the practical output electric energy is enough to prepare the consumed acid and alkali by electrolysis of water as aforementioned discussion. The alkaline-acidic design can achieve at least an extra 0.83 V electrochemical driving force at 1 M alkaline anoltye and 1 M acidic catholyte. Thus, the LFFC can obtain positive energy output only when the output voltage is greater than 0.83 V. We further investigated a relatively long-term discharging test at constant voltage of 0.9 V (with 1 M alkaline anolyte and 1 M acidic catholyte). During an 8-h discharging, 1327 C electrons were collected, corresponding to net energy produced by the LFFC of (0.9–0.83)× 1327 = 92.9 J. This result indicates that the electric energy output by the LFFC can exceed the neutralization energy caused by the consumption of OH^- and H^+. Therefore, to sum up, neutralization reaction indeed occurs in this system. If no lignin is present in the anolyte, OER takes place on the anode, namely that the electrochemical neutralization can be converted to electric energy by the LFFC. However, if lignin is present in the system, OER is significantly inhibited. The theoretical electric energy produced by complete oxidation of lignin is much larger than the neutralization energy, and the LFFC shows positive energy output in a practical application. Thus, the developed LFFC in this work might be promising for coupling alkaline waste water treatment and electricity generation by oxidation of the organic pollutants such as lignin.

4. Conclusions

Metal sulfide was loaded on Ni foam by electro-deposition as an electrocatalyst to promote the oxidation of lignin on anode for efficient and direct conversion of lignin to electricity by LFFCs under mild conditions. CoS has been screened as an efficient anodic catalyst to promote electron transfer from lignin. When VO^{2+}/VO_2^+ redox couple was used as the cathodic electron mediators under the catalysis of nitric acid, exciting power density was obtained. By optimizing the operational parameters for discharging, the highest peak power density of 176 mW/cm^2 was achieved with sodium lignosulfonate as the fuel. However, this LFFC showed good versatility to convert various fuels including phenols and aromatic aldehydes to electricity. The anode showed relatively good stability for at least four fed-batch operations without significant loss of the activity with an anodic efficiency of 97%. Lignin underwent significant depolymerization and degradation on the CoS@Ni anode primarily by oxidative cleavage of β-O-4′ aryl ether bond, while ring-opening reactions also took place to form aliphatic acids, and even a part of lignin was mineralized to CO_2. This work thus can provide a new LFFC technology for efficiently converting lignin to electricity, and may be applied in treatment of pulping mill waste water coupling with waste-to-power conversion.

CRediT authorship contribution statement

Denghao Ouyang: Investigation, Methodology, Formal analysis, Writing – original draft; **Daihong Gao:** Investigation, Methodology, Validation; **Ye Qiang:** Resources, Validation; **Xuebing Zhao:** Conceptualization, Supervision, Writing – review & editing, Funding acquisition, Project administration.

Declaration of Competing Interest

The authors declare that they have no known competing financial interests or personal relationships that could have appeared to influence the work reported in this paper.

Data Availability

Data will be made available on request.

Acknowledgements

This work was supported by the National Natural Science Foundation of China (No. 22178197).

Appendix A. Supporting information

Supplementary data associated with this article can be found in the online version at doi:10.1016/j.apcatb.2023.122491.

References

[1] Z.Y. Zhou, D.H. Liu, X.B. Zhao, Conversion of lignocellulose to biofuels and chemicals via sugar platform: an updated review on chemistry and mechanisms of acid hydrolysis of lignocellulose, Renew. Sust. Energ. Rev. 146 (2021), 111169, https://doi.org/10.1016/j.rser.2021.111169.

[2] F.Q. Wang, D.H. Ouyang, Z.Y. Zhou, S.J. Page, D.H. Liu, X.B. Zhao, Lignocellulosic biomass as sustainable feedstock and materials for power generation and energy storage, J. Energy Chem. 57 (2021) 247–280, https://doi.org/10.1016/j.jechem.2020.08.060.

[3] D.H. Ouyang, F.Q. Wang, H.S. Yang, X.B. Zhao, Haze to electricity: efficiently harvesting electric energy from air pollutants by construction of bioinspired electron transport chains in light- and heat-driven liquid flow fuel cells, Chem. Eng. J. 420 (2021) 129716–129730, https://doi.org/10.1016/j.cej.2021.129716.

[4] W. Liu, W. Mu, M.J. Liu, X.D. Zhang, H.L. Cai, Y.L. Deng, Solar-induced direct biomass-to-electricity hybrid fuel cell using polyoxometalates as photocatalyst and charge carrier, Nat. Commun. 5 (2014) 8, https://doi.org/10.1038/ncomms4208.

[5] H.S. Yang, Y.C. Bai, D.H. Ouyang, F.Q. Wang, D.H. Liu, X.B. Zhao, Coupling biomass pretreatment for enzymatic hydrolysis and direct biomass-to-electricity conversion with molybdovanadophosphoric heteropolyacids as anode electron transfer carriers, J. Energy Chem. 58 (2021) 133–146, https://doi.org/10.1016/j.jechem.2020.09.009.

[6] W. Liu, Y.T. Gong, W.B. Wu, W.S. Yang, C.M. Liu, Y.L. Deng, Z.S. Chao, Efficient biomass fuel cell powered by sugar with photo- and thermal-catalysis by solar irradiation, ChemSusChem 11 (2018) 2229–2238, https://doi.org/10.1002/cssc.201800719.

[7] H.H. Weetal, B.D. Forsyth, W.J.B. Hertl, Bioengineering, a direct fuel cell for the production of electricity from lignin, Biotechnol. Bioeng. 27 (1985) 972–979, https://doi.org/10.1002/bit.260270707.

[8] Y.A. Chen, H.S. Yang, D.H. Ouyang, T.X. Liu, D.H. Liu, X.B. Zhao, Construction of electron transfer chains with methylene blue and ferric ions for direct conversion of lignocellulosic biomass to electricity in a wide pH range, Appl. Catal. B Environ. 265 (2020) 13, https://doi.org/10.1016/j.apcatb.2019.118578.

[9] X. Liu, M. Hao, M. Feng, L. Zhang, Y. Zhao, X. Du, G. Wang, A one-compartment direct glucose alkaline fuel cell with methyl viologen as electron mediator, Appl. Energy 106 (2013) 176–183, https://doi.org/10.1016/j.apenergy.2013.01.073.

[10] X.H. Zu, L.L. Sun, J. Gong, X.C. Liu, Y.X. Liu, X. Du, W. Liu, L.F. Chen, G.B. Yi, W. G. Zhang, W.J. Lin, W.Z. Li, Y.L. Deng, Ferric ion pair mediated biomass redox flow fuel cell and related chemical reaction kinetics study, Chem. Eng. J. 348 (2018) 476–484, https://doi.org/10.1016/j.cej.2018.03.190.

[11] D. Ouyang, F. Wang, J. Hong, D. Gao, X. Zhao, Ferricyanide and vanadyl (V) mediated electron transfer for converting lignin to electricity by liquid flow fuel cell with power density reaching 200 mW/cm^2, Appl. Energy 304 (2021), 117927, https://doi.org/10.1016/j.apenergy.2021.117927.

[12] F. Xu, H. Li, Y.L. Liu, Q. Jing, Advanced redox flow fuel cell using ferric chloride as main catalyst for complete conversion from carbohydrates to electricity, Sci. Rep. 7 (2017) 9, https://doi.org/10.1038/s41598-017-05535-2.

[13] X.H. Zu, Z.H. Yang, L.L. Sun, W.J. Lin, G.B. Yi, X.Q. Zheng, W.Z. Li, Y.L. Deng, J. Xiao, Ferric-ferrous redox couple mediated low temperature symmetric flow fuel cell for direct conversion of biomass residues into electricity, J. Power Sources 448 (2020) 9, https://doi.org/10.1016/j.jpowsour.2019.227441.

[14] S.B. Han, D.H. Kwak, H.S. Park, I.A. Choi, J.Y. Park, S.J. Kim, M.C. Kim, S. Hong, K. W. Park, High-performance chemically regenerative redox fuel cells using a NO_3^-/NO regeneration reaction, Angew. Chem. Int. Ed. 56 (2017) 2893–2897, https://doi.org/10.1002/anie.201610738.

[15] X.B. Zhao, W. Liu, Y.L. Deng, J.Y. Zhu, Low-temperature microbial and direct conversion of lignocellulosic biomass to electricity: advances and challenges, Renew. Sust. Energ. Rev. 71 (2017) 268–282, https://doi.org/10.1016/j.rser.2016.12.055.

[16] W. Liu, W. Mu, Y.L. Deng, High-performance liquid-catalyst fuel cell for direct biomass-into-electricity conversion, Angew. Chem. Int. Ed. 53 (2014) 13558–13562, https://doi.org/10.1002/anie.201408226.

[17] J. Gong, W. Liu, X. Du, C.M. Liu, Z. Zhang, F.F. Sun, L. Yang, D. Xu, H. Guo, Y. L. Deng, Direct conversion of wheat straw into electricity with a biomass flow fuel vell mediated by two redox ion pairs, ChemSusChem 10 (2017) 506–513, https://doi.org/10.1002/cssc.201601441.

[18] Y. Tian, X. Liu, L. Xu, D. Yuan, Y. Dou, J. Qiu, H. Li, J. Ma, Y. Wang, D. Su, Engineering crystallinity and oxygen vacancies of Co (II) oxide nanosheets for high performance and robust rechargeable Zn–air batteries, Adv. Funct. Mater. 31 (2021) 2101239, https://doi.org/10.1002/adfm.202101239.

[19] L. Yan, Z. Xu, W. Hu, J. Ning, Y. Zhong, Y. Hu, Formation of sandwiched leaf-like CNTs-Co/ZnCo2O4@ NC-CNTs nanohybrids for high-power-density rechargeable Zn-air batteries, Nano Energy 82 (2021), 105710, https://doi.org/10.1016/j.nanoen.2020.105710.

[20] V.L. Singleton, R. Orthofer, R.M. Lamuela-Raventós, Analysis of total phenols and other oxidation substrates and antioxidants by means of folin-ciocalteu reagent. Methods in enzymology, Elsevier,, 1999, pp. 152–178, https://doi.org/10.1016/S0076-6879(99)99017-1.

[21] E.A. Ainsworth, K.M. Gillespie, Estimation of total phenolic content and other oxidation substrates in plant tissues using Folin–Ciocalteu reagent, Nat. Protoc. 2 (2007) 875–877, https://doi.org/10.1038/nprot.2007.102.

[22] R. Barik, P.P. Ingole, Challenges and prospects of metal sulfide materials for supercapacitors, Curr. Opin. Electrochem 21 (2020) 327–334, https://doi.org/10.1016/j.coelec.2020.03.022.

[23] Q. Liu, X. Hong, X. You, X. Zhang, X. Zhao, X. Chen, M. Ye, X. Liu, Designing heterostructured metal sulfide core-shell nanoneedle films as battery-type electrodes for hybrid supercapacitors, Energy Stor. Mater. 24 (2020) 541–549, https://doi.org/10.1016/j.ensm.2019.07.001.

[24] Y.C. Ding, P.W. Cai, Z.H. Wen, Electrochemical neutralization energy: from concept to devices, Chem. Soc. Rev. 50 (2021) 1495–1511, https://doi.org/10.1039/d0cs01239d.

[25] S. Adhikari, Y. Kwon, D.-H. Kim, Three-dimensional core–shell structured NiCo2O4@ CoS/Ni foam electrocatalyst for oxygen evolution reaction and electrocatalytic oxidation of urea, Chem. Eng. J. 402 (2020), 126192, https://doi.org/10.1016/j.cej.2020.126192.

[26] B. Liu, S. Qu, Y. Kou, Z. Liu, X. Chen, Y. Wu, X. Han, Y, In situ electrodeposition of cobalt sulfide nanosheet arrays on carbon cloth as a highly efficient bifunctional electrocatalyst for oxygen evolution and reduction reactions, ACS Appl. Mater. Interfaces 10 (2018) 30433–30440, https://doi.org/10.1021/acsami.8b10645.

[27] K. Lejaeghere, V. Van Speybroeck, G. Van Oost, S. Cottenier, Error estimates for solid-state density-functional theory predictions: an overview by means of the ground-state elemental crystals, Crit. Rev. Solid State Mater. Sci. 39 (2014) 1–24, https://doi.org/10.1080/10408436.2013.772503.

[28] P. Zhang, X. Sheng, X. Chen, Z. Fang, J. Jiang, M. Wang, F. Li, L. Fan, Y. Ren, B. Zhang, Paired electrocatalytic oxygenation and hydrogenation of organic substrates with water as the oxygen and hydrogen source, Angew. Chem. Int. Ed. 131 (2019) 9253–9257, https://doi.org/10.1002/ange.201903936.

[29] B. Zhu, C. Chen, L. Huai, Z. Zhou, L. Wang, J. Zhang, 2, 5-Bis (hydroxymethyl) furan: a new alternative to HMF for simultaneously electrocatalytic production of FDCA and H2 over CoOOH/Ni electrodes, Appl. Catal. B Environ. 297 (2021), 120396, https://doi.org/10.1016/j.apcatb.2021.120396.

[30] A. Toledano, L. Serrano, J. Labidi, Organosolv lignin depolymerization with different base catalysts, J. Chem. Technol. Biotechnol. 87 (2012) 1593–1599, https://doi.org/10.1002/jctb.3799.

[31] A.E. Kazzaz, P. Fatehi, Technical lignin and its potential modification routes: a mini-review, Ind. Crops Prod. 154 (2020), 112732, https://doi.org/10.1016/j.indcrop.2020.112732.

[32] J. Haber, J. Stoch, L. Ungier, X-ray photoelectron spectra of oxygen in oxides of Co, Ni, Fe and Zn, J. Electron Spectros Relat. Phenom. 9 (1976) 459–467, https://doi.org/10.1016/0368-2048(76)80064-3.

[33] H. Zhou, Y. Ren, Z. Li, M. Xu, Y. Wang, R. Ge, X. Kong, L. Zheng, H. Duan, Electrocatalytic upcycling of polyethylene terephthalate to commodity chemicals and H_2 fuel, Nat. Commun. 12 (2021) 1–9, https://doi.org/10.1038/s41467-021-25048-x.

[34] D.W. Wakerley, M.F. Kuehnel, K.L. Orchard, K.H. Ly, T.E. Rosser, E. Reisner, Solar-driven reforming of lignocellulose to H2 with a CdS/CdO_x photocatalyst, Nat. Energy 2 (2017) 1–9, https://doi.org/10.1038/nenergy.2017.21.

[35] X.B. Zhao, J.L. Wen, H.M. Chen, D.H. Liu, The fate of lignin during atmospheric acetic acid pretreatment of sugarcane bagasse and the impacts on cellulose enzymatic hydrolyzability for bioethanol production, Renew. Energy 128 (2018) 200–209, https://doi.org/10.1016/j.renene.2018.05.071.

[36] R. Ma, Y. Xu, X. Zhang, Catalytic oxidation of biorefinery lignin to value-added chemicals to support sustainable biofuel production, ChemSusChem 8 (2015) 24–51, https://doi.org/10.1002/cssc.201402503.

[37] T. Shiraishi, T. Takano, H. Kamitakahara, F. Nakatsubo, Studies on electrooxidation of lignin and lignin model compounds. Part 1: direct electrooxidation of non-phenolic lignin model compounds, Holzforschung 66 (2012) 311–315, https://doi.org/10.1515/hf.2011.140.

[38] C. Yang, S. Maldonado, C.R. Stephenson, Electrocatalytic lignin oxidation, ACS Catal. 11 (2021) 10104–10114, https://doi.org/10.1021/acscatal.1c01767.

[39] Z. Sun, B. Fridrich, A. De Santi, S. Elangovan, K. Barta, Bright side of lignin depolymerization: toward new platform chemicals, Chem. Rev. 118 (2018) 614–678, https://doi.org/10.1021/acs.chemrev.7b00588.

[40] T. Hibino, K. Kobayashi, M. Nagao, S. Teranishi, Hydrogen production by direct lignin electrolysis at intermediate temperatures, ChemElectroChem 4 (2017) 3032–3036, https://doi.org/10.1002/celc.201700917.

[41] Y. Mardiyati, E.Y. Tarigan, P. Prawisudha, S.Ma Shoimah, R.R. Rizkiansyah, S. Steven, Binderless, all-lignin briquette from black liquor waste: isolation, purification, and characterization, Molecules 26 (2021) 650, https://doi.org/10.3390/molecules26030650.

[42] D. Bajwa, G. Pourhashem, A.H. Ullah, S. Bajwa, A concise review of current lignin production, applications, products and their environmental impact, Ind. Crops Prod. 139 (2019), 111526, https://doi.org/10.1016/j.indcrop.2019.111526.

[43] O. Muneeb, I. Chino, A. Saenz, J.L. Haan, An ascorbate fuel cell with carbon black nanoparticles as anode and cathode, J. Power Sources 413 (2019) 216–221, https://doi.org/10.1016/j.jpowsour.2018.12.042.

[44] W.A. Shewa, J.A. Lalman, S.R. Chaganti, D.D. Heath, Electricity production from lignin photocatalytic degradation byproducts, Energy 111 (2016) 774–784, https://doi.org/10.1016/j.energy.2016.05.007.

[45] H. Bermek, T. Catal, Y. Fan, H. Liu, A clean technology to convert sucrose and lignocellulose in microbial electrochemical cells into electricity and hydrogen, Bioresour. Technol. Rep. 5 (2019) 331–334, https://doi.org/10.1016/j.biteb.2018.10.002.

[46] R.C. Oliveira, M.J. Jeremias, M.M. Mateus, D.M. Santos, Developing a novel direct liquid fuel cell based on pulping liquors, Fuel Cells 22 (2022) 39–47, https://doi.org/10.1002/fuce.202100109.
[47] T. Hibino, K. Kobayashi, P. Lv, M. Nagao, S. Teranishi, T. Mori, An intermediate-temperature biomass fuel cell using wood sawdust and pulp directly as fuel, J. Electrochem. Soc. 164 (2017) F557, https://doi.org/10.1149/2.0511706jes.
[48] T. Hibino, K. Kobayashi, S. Teranishi, T. Hitomi, Solid oxide fuel cell using municipal solid waste directly as fuel: biomass, resin, plastic, and food waste, ACS Sustain. Chem. Eng. 9 (2021) 3124–3136, https://doi.org/10.1021/acssuschemeng.0c07657.
[49] Y. Xie, J. Xiao, Q. Liu, X. Wang, J. Liu, P. Wu, S. Ouyang, Highly efficient utilization of walnut shell biochar through a facile designed portable direct carbon solid oxide fuel cell stack, Energy 227 (2021), 120456, https://doi.org/10.1016/j.energy.2021.120456.
[50] R.B. Lima, R. Raza, H. Qin, J. Li, M.E. Lindström, B. Zhu, Direct lignin fuel cell for power generation, RSC Adv. 3 (2013) 5083–5089, https://doi.org/10.1039/C3RA23418E.
[51] N. Jafri, W. Wong, L. Yoon, K. Cheah, Pretreated mesocarp fibre biochars as carbon fuel for direct carbon fuel cells, Int. J. Hydrog. Energy 46 (2021) 16762–16775, https://doi.org/10.1016/j.ijhydene.2020.09.034.
[52] W. Cai, X. Tong, X. Yan, H. Li, Y. Li, X. Gao, Y. Guo, W. Wu, D. Fu, X. Huang, Direct carbon solid oxide fuel cells powered by rice husk biochar, Int. J. Energy Res. 46 (2022) 4965–4974, https://doi.org/10.1002/er.7489.
[53] W. Hao, P. Luo, Z. Wu, Y. Mi, Z. Gao, The effect of biomass pyrolysis temperature on the performance of biochar-fed molten hydroxide direct carbon fuel cells, Biomass Bioenergy 150 (2021), 106122, https://doi.org/10.1016/j.biombioe.2021.106122.
[54] W. Hao, P. Luo, Z. Wu, G. Sun, Y. Mi, Feasibility of pine bark pellets and their pyrolyzed biochar pellets as fuel sources in molten hydroxide direct carbon fuel cells, Energy Fuels 34 (2020) 16756–16764, https://doi.org/10.1021/acs.energyfuels.0c03171.
[55] Y. Liu, D. Ning, L. Zheng, Q. Zhang, L. Gu, R. Gao, J. Zhang, A. Franz, G. Schumacher, X. Liu, Improving the electrochemical performances of Li-rich $Li_{1.20}Ni_{0.13}Co_{0.13}Mn_{0.54}O_2$ through a cooperative doping of Na^+ and PO_4^{3-} with Na_3PO_4, J. Power Sources 375 (2018) 1–10, https://doi.org/10.1016/j.jpowsour.2018.02.040.
[56] A. Elleuch, K. Halouani, Y. Li, Investigation of chemical and electrochemical reactions mechanisms in a direct carbon fuel cell using olive wood charcoal as sustainable fuel, J. Power Sources 281 (2015) 350–361, https://doi.org/10.1016/j.jpowsour.2015.01.171.